ORNL/TM-11392

MARTIN MARIETTA ENERGY SYSTEMS LIBRARIES

3 4456 0319787 7

ornl

OAK RIDGE
NATIONAL
LABORATORY

MARTIN MARIETTA

Advances in Iridium Alloy Processing in FY 1988

E. K. Ohriner
R. L. Heestand

OAK RIDGE NATIONAL LABORATORY
CENTRAL RESEARCH LIBRARY
CIRCULATION SECTION
4500N ROOM 175
LIBRARY LOAN COPY
DO NOT TRANSFER TO ANOTHER PERSON
If you wish someone else to see this report, send in name with report and the library will arrange a loan.

OPERATED BY
MARTIN MARIETTA ENERGY SYSTEMS, INC.
FOR THE UNITED STATES
DEPARTMENT OF ENERGY

This report has been reproduced directly from the best available copy.

Available to DOE and DOE contractors from the Office of Scientific and Technical Information, P.O. Box 62, Oak Ridge, TN 37831; prices available from (615) 576-8401, FTS 626-8401.

Available to the public from the National Technical Information Service, U.S. Department of Commerce, 5285 Port Royal Rd., Springfield, VA 22161.
NTIS price codes—Printed Copy: A04 Microfiche A01

This report was prepared as an account of work sponsored by an agency of the United States Government. Neither the United States Government nor any agency thereof, nor any of their employees, makes any warranty, express or implied, or assumes any legal liability or responsibility for the accuracy, completeness, or usefulness of any information, apparatus, product, or process disclosed, or represents that its use would not infringe privately owned rights. Reference herein to any specific commercial product, process, or service by trade name, trademark, manufacturer, or otherwise, does not necessarily constitute or imply its endorsement, recommendation, or favoring by the United States Government or any agency thereof. The views and opinions of authors expressed herein do not necessarily state or reflect those of the United States Government or any agency thereof.

ORNL/TM-11392
Distribution
Category UC-504

Metals and Ceramics Division

ADVANCES IN IRIDIUM ALLOY PROCESSING IN FY 1988

E. K. Ohriner and R. L. Heestand

Date Published - December 1989

Prepared for
DOE Office of Space and Defense Power Systems,
Office of Special Applications
AF 70 10 20 0

Prepared by the
OAK RIDGE NATIONAL LABORATORY
Oak Ridge, Tennessee 37831-6285
operated by
MARTIN MARIETTA ENERGY SYSTEMS, INC.
for the
U.S. DEPARTMENT OF ENERGY
under Contract No. DE-AC05-84OR21400

MARTIN MARIETTA ENERGY SYSYEMS LIBRARIES

3 4456 0319787 7

CONTENTS

LIST OF TABLES v
LIST OF FIGURES vii
ABSTRACT 1
1. INTRODUCTION 2
2. BACKGROUND 3
3. ARC-MELTING DEVELOPMENT 4
3.1 ARC-MELTING EXPERIMENTS WITH STAINLESS STEEL 4
3.1.1 Purpose of Simulations 4
3.1.2 Effects of Argon Backfill and Mold Condition 5
3.1.3 Effect of Arc Current 5
3.1.4 Effects of Electrode Alignment and Mold Diameter 6
3.1.5 Effect of Vacuum Pressure 9
3.2 CONSUMABLE ARC MELTING OF SCRAP IRIDIUM ALLOY INGOTS 12
3.2.1 Arc Melting of the RS1 Electrode 12
3.2.2 Arc Melting of the RS2 Electrode 15
3.2.3 Arc Melting of the RS3 Electrode 16
4. PROCESSING OF IRIDIUM ALLOY INGOTS 21
4.1 PROCESSING OF BR6 BLANKS 21
4.2 PROCESSING OF C1 BLANKS 22
4.3 PROCESSING OF D1 INGOTS 24
4.3.1 D1 Electrode Preparation 24
4.3.2 D1 Arc Melting and Ingot Preparation 25
4.3.3 D1 Extrusion and Rolling 26
4.3.4 D1 Blank Inspection 34
4.4 PROCESSING OF E1 INGOT 35
4.4.1 E1 Electrode Preparation 35
4.4.2 E1 Arc Melting and Ingot Preparation 37
5. MATERIALS USAGE IN ALLOY BLANK PROCESSING 42
6. SUMMARY 47
6.1 DISCUSSION 47
6.2 RECOMMENDATIONS 48

7. ACKNOWLEDGMENTS 48
8. REFERENCES 49

LIST OF TABLES

Table 1. Summary of yields for blanks produced since FY 1984 3

Table 2. Arc melting of stainless steel in 51-mm-diam mold with varying mold surface conditions..... 6

Table 3. Clearances between electrode and wall of 63-mm-diam mold for melt 25 8

Table 4. Effect on ingot surface appearance of clearance between electrode and mold wall 9

Table 5. Summary of vacuum arc-melting simulations with stainless steel.....10

Table 6. Distribution of blisters in recrystallized sheets and rejected blanks from C1 ingot 23

Table 7. Result of ultrasonic inspection of blanks from D1 ingot 34

Table 8. Materials balance for E1 electrode fabrication 42

Table 9. Materials balance for E1 arc-melting and ingot preparation 43

Table 10. Materials balance for blank preparation from D1 extrusion.....44

Table 11. Summary of estimated residual scrap recoveries and losses.....45

Table 12. Predicted materials balance for blank production 46

LIST OF FIGURES

Fig. 1. Plot of melting parameters for arc melting of stainless steel in a 51-mm-diam mold with step change in applied current (melt 20) 7

Fig. 2. Plot of melting parameters for arc melting of stainless steel in a 51-mm-diam mold in vacuum (melt 41) 11

Fig. 3. Plot of melting parameters for arc melting of stainless steel in a 51-mm-diam mold using argon backfill (melt 32) 12

Fig. 4. Melt data plot for refinable scrap DOP-26 melt, RS1 13

Fig. 5. Cast RS1 ingot and electrode stub shows evidence of intermittent arcing to mold wall 14

Fig. 6. Plot of arc current, arc voltage, and electrode position for RS2 iridium alloy refinable-scrap ingot melted in a 54-mm-diam mold 16

Fig. 7. DOP-26 iridium alloy refinable-scrap arc-melted ingot (54-mm diam). Front view of RS2 ingot 17

Fig. 8. DOP-26 iridium alloy refinable-scrap arc-melted ingot (63-mm diam). Front view of RS3 ingot 19

Fig. 9. Pore on the surface of arc-melted RS3 iridium alloy ingot. A generally smooth melted surface is seen at the base of the pore with ripples on the melted surface. These are associated with a nonuniform solidification rate. Magnification: 16X 20

Fig. 10. Plot of arc current, arc voltage, and electrode position for RS3 iridium alloy refinable-scrap ingot melted in a 63-mm-diam mold 21

Fig. 11. Cross section through a blister in sheet C1-7 following recrystallization at 1300°C shows a large subsurface defect 23

Fig. 12. Plot of arc current, arc voltage, and electrode position during arc melting of D1 iridium alloy electrode 25

Fig. 13. Arc-melted D1 iridium alloy ingot and electrode stub 27

Fig. 14. Iridium alloy ingot D1 following surface grinding and dye-penetrant inspection 28

Fig. 15. Microstructure of D1 bar extruded at 1325°C. Longitudinal section from nose portion of bar 30

Fig. 16. Microstructure of D1 bar extruded at 1325°C. Longitudinal section from center portion of bar 31

Fig. 17. Microstructure of D1 bar extruded at 1325°C. Longitudinal section from tail portion of bar 32

Fig. 18. Microstructure of B2 bar extruded at 1250°C. Longitudinal section from tail portion of bar 33

Fig. 19. Weight losses during electron beam melt refining of the four batch blends used for E1 electrode 36

Fig. 20. Results on inspection of E1-welded electrode by electrical conductance measurements 38

Fig. 21. Plot of arc current, arc voltage, and electrode position for E1 iridium alloy ingot melted in a 63-mm-diam mold 39

Fig. 22. E1 ingot vacuum arc melted in 63-mm-diam mold. The skull of unremelted splatter at top of the ingot is larger than other iridium ingots. The surface quality is considerably improved over the smaller diameter D1 ingot 40

Fig. 23. E1 ingot, after grinding to 61.5-mm diam 41

ADVANCES IN IRIDIUM ALLOY PROCESSING IN FY 1988*

E. K. Ohriner and R. L. Heestand

ABSTRACT

A new process for the production of DOP-26 iridium alloy blanks is being evaluated and optimized. The alloy is prepared by electron-beam (EB) melting of Ir-0.3% W powder compacts followed by doping with aluminum and thorium by arc melting. Drop-cast alloy rod segments are EB welded together into an electrode that is arc melted to produce an ingot for extrusion and subsequent sheet rolling and blanking. Initial results showed rejections for ultrasonic indications for alloy blanks fabricated by this process to be very low. Subsequently, some ingots have exhibited delaminations in the sheet, leading to blank rejection rates similar to that obtained in the standard process. The occurrence of ultrasonic indications in the blanks are now shown to be associated with the presence of subsurface flaws in the arc-melted ingot that are not healed during extrusion or the subsequent rolling of the sheet. There is substantial evidence indicating that the occurrence of surface and subsurface flaws in the ingots are exacerbated by the relatively small clearances between he electrode and the side wall of the 51-mm-diam mold. These results obtained from experi-mental melts, with both stainless steel and scrap iridium alloy materials, have led to a recommendation for arc melting in a large 63-mm-diam mold. The fabrication of blanks from this larger diameter ingot is under way. The efficiency of iridium material utilization in the new process is also discussed.

---

1. INTRODUCTION

This report deals with progress made during 1988 in iridium alloy sheet and blank processing, using a new manufacturing process, namely, a consumable arc-melting, extruding, and rolling procedure. The objectives of the 1988 activities included (1) identification of laboratory capabilities for the new process and problems associated with this process; (2) continuation of process optimization and procedure modifications; (3) resolution of processing problems; (4) maintenance of blank production capability, including critical staff availability; and (5) coordination of new process qualification efforts.

*Research sponsored by the Office of Space and Defense Power Systems, Office of Special Applications, U.S. Department of Energy, under contract DE-AC05-84OR21400 with Martin Marietta Energy Systems, Inc.

The new process for production, rather than using nonconsumable arc melting and drop casting of small (500-g) ingots for rolling, uses the drop-cast ingots to fabricate an electrode for consumable arc melting into a large (10-kg) ingot.[1] This ingot is extruded to a rectangular bar for rolling to sheet or foil. The new process offers the potential for a significant reduction in unit blank production cost through both improved yields and reduced labor costs. The increase in the number of blanks per ingot leads to a reduction in manufacturing work-hours per blank and a decrease in the number of chemical analyses performed. The casting of large ingots, which do not require weld repair, and the use of the extrusion process can increase processing yields through a substantial reduction in laminar defects and ultrasonic indication rejection. The results obtained on the first two ingots processed to blanks showed a substantial decrease in blank rejection rate for ultrasonic-detected defects. Although these high yields were not reproduced with several subsequently processed ingots,[2] in all cases blank yields were equal to those previously achieved in the standard production process.

In order to achieve reproducible high yields, we have made a major effort to improve the quality of the consumable arc-melted ingots. The quality has been evaluated by nondestructive evaluation (NDE) of the ground ingots prior to extrusion. The results from the NDE were used to orient the ingot during extrusion so that the internal defects and near-surface defects are located as much as possible where they will have the least influence on the finished blanks. A study of several consumable arc-melting parameters using both stainless steel and scrap iridium has led to a better understanding of the effect of melting parameters on the occurrence of both surface and subsurface defects in the arc-melted ingots. The results of these experiments are described in this report. They form the basis of the present effort to increase the mold diameter from 51 mm to 63 mm. The work with the larger mold is described through the arc-melting operation. Furthermore, several shortcomings of the existing arc-melting furnace have been found to interfere with the consistent production of high-quality ingots. Authorization has been obtained for the purchase of a new automated furnace with improved electrode alignment and arc-gap control.

The efficiency of iridium material utilization in the new process has been evaluated. Estimates of the generation and usage of iridium alloy recycle material, the recovery of iridium scrap, and the loss of iridium have been made for the various processing steps.

2. BACKGROUND

Demonstration of the new consumable arc-melting and extruding process was initiated in FY 1984 for DOP-26 alloy (Ir-0.3% W-O.006% Th-0.005% Al). A consumable arc-melted DOP-26 alloy ingot (designated AC) was made, cut into two 19- × 19- × 54-mm ingots, and rolled into sheets using the standard rolling process. Blanks cut from these sheets were found to be free of both ultrasonic- and penetrant-detected defects. In FY 1985, new process development was continued by arc melting two consumable electrodes (B1 and B2), which were then extruded to rectangular bars, cut into billets, and rolled into sheets using a procedure modified for extruded material. Blanks cut from the B1 and B2 sheets were also found to be free of penetrant- and ultrasonic-detected defects, giving a yield of greater than 95% acceptance. A third ingot, produced from recycled material and designated BR3, was later found to be contaminated with molybdenum. Changes were implemented in the recycling practice to avoid use of contaminated scrap. During FY 1986, an additional ingot (B4) was processed to sheets. Results of blank inspection showed rejection of 15 of 43 blanks for ultrasonic-detected defects. During FY 1987, another ingot (B5) was processed to blanks; of these, 11 of 42 machined blanks were rejected, as was sheet material equivalent to an additional 7 blanks found defective by ultrasonic inspection. The yields of blanks at NDE for these new process ingots, as well as for the most recent standard process ingots (XR and ZR), are summarized in Table 1.

Table 1. Summary of yields for blanks produced since FY 1984

Ingot identity	No. of ingots	Potential blanks	Defective sheet-equivalent blanks[a]	Machined blanks	No. of deliverable blanks	Yield	
						From sheet (%)	From blanks (%)
XR	18	108	25	83	68	63	82
ZR	12	72	14	58	39	54	67
B1	1	46	0	42[b]	42	100	100
B2	1	46	0	39[c]	39	100	100
B4	1	50	7	43	28	56	65
B5	1	54	12	42	31	57	74
BR6	1	75	12	63	42	56	67

[a]Ultrasonic inspection of sheets.
[b]Sheet material equivalent to four blanks was used for tensile test specimens.
[c]Sheet material equivalent to seven blanks used for mechanical test specimens.

3. ARC-MELTING DEVELOPMENT

The consumable arc melting of the iridium alloy ingots is believed to be an important cause of laminant defects in the rolled sheet and finished blanks. Small pores in the ingot are likely to result in laminar defects following rolling. The location of the defects, which are commonly found in bands extending the length of several blanks and which frequently extend through more than one rolled sheet, strongly suggests that the defects are initiated prior to rolling. Furthermore, the arc-melted ingots have shown significant variability in surface appearance, indicating incomplete control of the melting parameters. In order to establish the important arc-melting parameters, we studied the arc-melting process using both stainless steel and scrap iridium alloy.

3.1 ARC-MELTING EXPERIMENTS WITH STAINLESS STEEL

3.1.1 Purpose of Simulations

There are a large number of arc-melting parameters that can influence the surface and subsurface structure of the melted ingot. In order to evaluate the effects of these variables on the ingot surface quality, we performed several experimental melts, using stainless steel to conserve iridium. On the basis of these results, we then performed a much smaller number of experimental melts using iridium refinable-scrap material, as described later. The melt variables examined using the stainless steel simulation were (1) use of argon backfill, (2) mold surface condition, (3) arc current, (4) electrode alignment, (5) mold size, (6) electrode arc gap, and (7) vacuum chamber pressure. In evaluating these simulations, we recognized that there would be limitations on applying the results to the arc melting of iridium alloy because of differences in melting behavior of the two materials, the most important difference being the melting range of type 304L stainless steel, approximately 1440 to 1480°C, as compared to 2440 to 2445°C for DOP-26 iridium alloy. Other potentially important differences include the vapor pressure of the materials, the surface tension of the liquids, the oxidation behavior at low oxygen pressures, and the presence of pores and weld defects in the fabricated iridium electrode. Nevertheless, we obtained much useful information from the stainless steel simulations.

3.1.2 Effects of Argon Backfill and Mold Condition

An initial series of seven melts were performed to evaluate the effect of a partial pressure of argon as compared to vacuum melting, as well as the effect of mold surface condition. Four stainless steel electrodes 25 mm in diameter were arc melted into 51-mm-diam molds under an argon backfill pressure of 68 kPa (0.66 atm). The arc gap appeared to be well controlled, and diffuse arcing or corona was not observed during these melts. The mold surfaces used included a new polished copper mold, a mold that had been used previously and had a tarnished surface, and a mold with a new polished surface that had been oxidized for 1 h at 400°C. In all cases, there was evidence of stainless steel, which appeared to fuse to the copper mold, and evidence of unremelted splatter on the ingot surface. There was no indication that an oxidized mold surface was effective in decreasing the local adherence of the stainless steel to the mold. The height of the skull on the top of the ingot was typically about 6 mm. The melted surfaces of the electrode stubs were nearly flat and perpendicular to the electrode axis, indicating good arc control. One melt was performed using an argon backfill pressure of 34 kPa (0.33 atm). At this pressure, the arc-gap control mechanism, which maintains a constant arc voltage, could not provide a constant arc gap. Two melts were performed under vacuum. The surface of these ingots showed more tarnishing than was seen for the ingots melted with an argon backfill and also exhibited larger surface defects. The skull heights of these ingots were about 4 cm, and the electrode stubs were rounded.

A summary of the melting parameters for this series of melts is shown in Table 2. The arc voltage ranged from 37 to 40 V for melts performed with an argon pressure of 68 kPa as compared to 34 V with a pressure of 34 kPa and 32 V in vacuum. The electrode feed rate is in a narrow range of 13.9 to 14.4 g/s. The same electrode feed rate is obtained in vacuum with a significantly lower arc current.

3.1.3 Effect of Arc Current

The surface appearance of stainless steel ingots melted under argon backfill in a 51-mm-diam mold was evaluated over a limited range of arc currents of 1800 to 2000 A in the melts described in the previous section. In order to evaluate the effect of arc current in a more direct way and investigate a larger range of currents, we melted a stainless steel electrode under an argon backfill in a 51-mm-diam mold with an initial current of 1800 A, which was reduced after 100 s to 1400 A and held at that level for an additional 100 s. The

Table 2. Arc melting of stainless steel in 51-mm-diam mold with varying mold surface conditions

Melt no.	Mold condition	Initial chamber pressure (Pa)	Arc voltage (V)	Arc current (A)	Average feed rate (g/s)
12	Used	$<10^{-2}$	32	2100	*a*
13	Used	3.4×10^4	34	2000	*a*
14	Used	6.8×10^4	40	1900	13.9
17	New, polished	6.8×10^4	37	1900	14.4
18	New, polished	6.8×10^4	39	1900	14.4
19	Polished and oxidized	6.8×10^4	39	1800	13.9
21	Polished and oxidized	7×10^{-3}	32	1600	14.4

[a]Irregular electrode feed.

recording of arc current, arc voltage, and electrode position is shown in Fig. 1. The electrode feed rate varied from 12.0 g/s at 1400 A to 13.8 g/s at 1800 A. The upper section of the ingot exhibited a more reflective surface than the lower surface, but the number and size of surface defects associated with arc strikes to the mold wall were similar for both halves of the ingot. There is no effect of arc current on ingot surface defects over the current range of 1400 to 2000 A.

3.1.4 Effects of Electrode Alignment and Mold Diameter

Observation of defects on the surfaces of a number of arc-cast stainless steel ingots suggested that they were associated with arc strikes to the copper mold at locations at or above the level of the splatter. Additional work was performed on characterizing and improving the alignment of the electrode within the mold and on evaluating the potential benefit of increased mold diameter. The aim of this work was to determine if the minimum clearance between the electrode and mold wall of 6.4 mm specified in the arc-melting procedure is sufficient.

A series of six stainless steel electrodes were melted into new or polished molds with diameters of either 51 or 63 mm with an argon backfill of 50 mPa. The arc voltage was maintained between 38 and 40 V and the arc current between 2000 and 2200 A. Prior to melting, the electrode was inserted in the electrode holder and transversed to full-up,

ORNL-DWG 89-19329

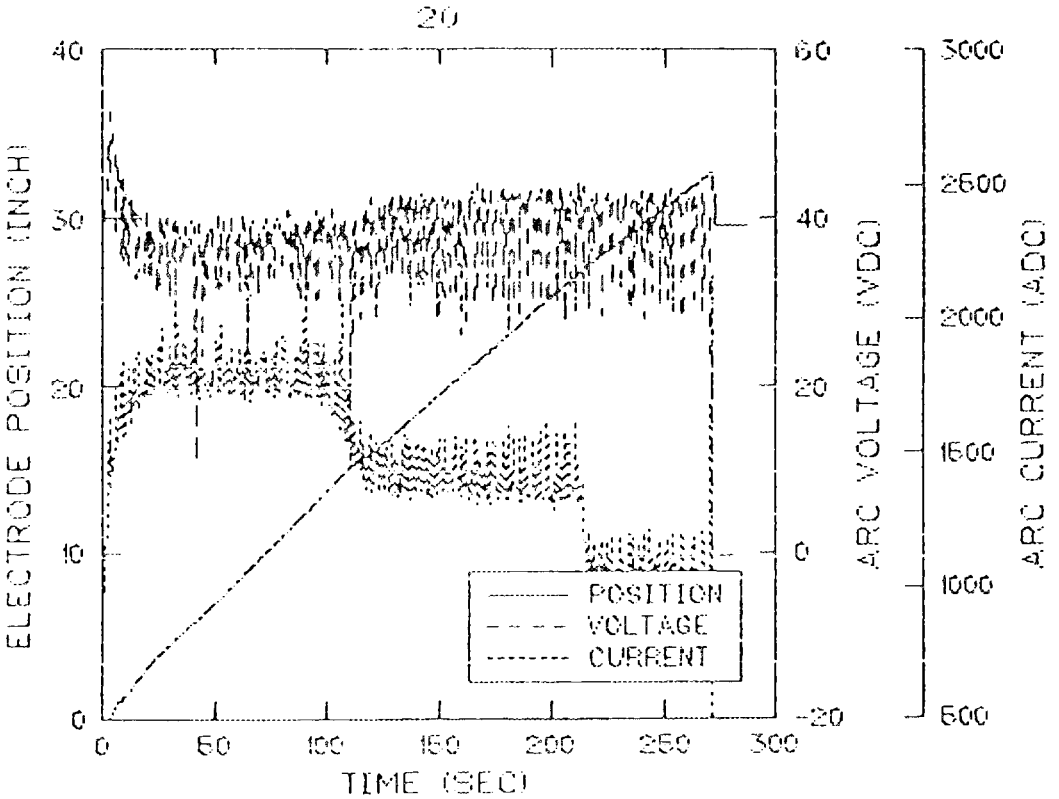

Fig. 1. Plot of melting parameters for arc melting of stainless steel in a 51-mm-diam mold with step change in applied current (melt 20).

midpoint, and full-down locations; and the clearance between the electrode and mold support flange was measured at each electrode location for positions spaced at equal angular increments around the flange. Since the mold is concentric with the flange, the clearances between the mold wall and the electrode may be calculated. The calculated clearances obtained for the first melt in the series (no. 25) with a 63-mm-diam mold are shown in Table 3. If the electrode feed is concentric with the mold, the clearance should be a constant 19 mm. The electrode is aligned at its midpoint but moves out of concentric alignment as the electrode holder moves up or down. Examination of the surface of the ingot obtained with this alignment showed no indications of arcing to the side wall over the bottom one-third of the ingot height, corresponding to the up position of the electrode. Severe surface defects were seen on the top one-third of the ingot, corresponding to the regions with clearances of 11 to 13 mm. Ingot surface defects were also observed, although to much lesser degree, in the middle third of the ingot, for which clearance values are 18 mm or more. Although not all ingot surface defects can be attributed to inadequate clearance between electrode and mold, it is clear that for this ingot, a clearance of less than 13 mm produces serious defects.

Table 3. Clearances (in mm) between electrode and wall of 63-mm-diam mold for melt no. 25 (calculated clearance at indicated electrode position)

Angular location (degree)	Before melting			After melting
	Up	Midpoint	Down	Down
60	17	18	18	17
120	15	19	25	25
180	18	20	27	27
240	21	20	20	21
300	23	19	13	13
360	20	19	11	11

On the basis of the above results, we evaluated a number of methods to improve electrode alignment. Modifications to the furnace to improve the electrode alignment were made. Specifically, two universal joints were placed between the electrode holder and the electrode drive support arm. This did result in an improved alignment. Further improvements in alignment, although desirable, would require a complete new electrode drive design. The existing furnace is 24 years old and was designed for melting of ingots 76 mm in diameter and larger. The main deficiency of electrode feed assembly is that it is not rigidly mechanically attached to the chamber. Major modifications to the equipment could not be justified in view of the age of the furnace. A capital expenditure for a new arc- melting furnace has been authorized, and specifications for the unit have been prepared.

In addition to mechanical methods of improving alignment of the electrode and the mold, two melts were performed in which the operator manually centered the electrode while the melt was in progress. This required sliding the upper cover of the vacuum chamber on its O-ring seals during melting. The first such melt was successful, but an air leak past the O-ring occurred during the second melt. This method of alignment was judged to be unreliable and was not pursued further.

Effects on the surface of arc melting six ingots with the different types of electrode alignment discussed above and with mold diameters of 51 and 63 mm are summarized in Table 4. The misalignment, measured as the difference between the mean clearance and the minimum clearance, was as large as ±9 mm for melt no. 25 using the old alignment and was reduced to ± 4 mm for melt no. 29 by a better centering procedure. Manual centering of melt no. 30 resulted in a misalignment of ±4 mm, as measured upon completion of the melt. The

Table 4. Effect on ingot surface appearance of clearance between electrode and mold wall

Melt no.	Mold diameter (mm)	Type of alignment	Calculated clearances (mm)			Ingot surface appearance
			Min	Max	Mean	
25	63	Old	10	27	19	One side good
27	63	Manual	---	---	19	Good
29	51	Old	10	17	13	One side good
30	63	Manual	16	23	19	Oxidized
31	51	Improved	11	14	13	One side good
32	51	Improved	11	15	13	One side good

improved type of alignment achieved misalignments of less than ±3 mm over the length of the electrode. The surface appearance of this series of ingots indicates that surface defects could generally be avoided when the minimum clearance between the electrode and mold is about 16 mm or greater. This is achieved with a well-aligned electrode and a 63-mm-diam mold. Surface defects could not be avoided in a 51-mm-diam mold because of the low clearance even for a well-aligned electrode.

The difficulties in arc melting a 51-mm-diam ingot are attributed to the small clearance between the electrode and the mold wall, a distance that may be less than the gap between the electrode and the molten pool. The length of the arc gap cannot be readily observed during melting and cannot be measured. It is possible, at least in principle, to vary the arc gap length by varying the voltage. The practical difficulty of a short arc is of extinguishing the arc and welding the electrode to the ingot.

3.1.5 Effect of Vacuum Pressure

After arc melting a substantial number of stainless steel electrodes and observing a substantial quantity of stainless steel splatter within the large vacuum chamber, we evaluated the effect of furnace-chamber pressure on the arc melting of stainless steel for the pressure range of 1 to 7 mPa. The accumulated splatter was believed to be acting as a virtual leak. The melt chamber was thoroughly cleaned and wire brushed, and the copper chamber liner was acid cleaned. In addition, a helium leak detector was used to locate small leaks. Use of these procedures resulted in a vacuum chamber pressure after overnight pumping of as low as 1 mPa, as compared to 7 mPa obtained with previous melts. Six stainless steel electrodes

were melted in vacuum, with initial pressures of 1 to 4 mPa and a chamber pressure during melting of 50 to 70 mPa. Mold diameters of both 51 and 63 mm were used, and arc currents ranged from 1200 to 2300 A. The melting conditions are sum-marized in Table 5. An exception to the low initial vacuum pressure occurred for melt no. 42, where a small leak in the sight glass O-ring seal caused the higher pressure of 9 mPa. The data for two earlier vacuum melts, nos. 12 and 21, are shown in Table 5 for comparison.

Table 5. Summary of vacuum arc-melting simulations with stainless steel

Melt no.	Mold diameter (mm)	Vacuum (mPa)		Arc current (A)	Electrode potential (V)	Average electrode feed rate (g/s)
		Before melt	During melt			
43	63	2	70	2000	31	20
42	51	9	50	1550	29	12
41	51	1	50	1550	28	15
40	51	--	---	---	---	---
39	51	4	50	2300	33	23
38	51	2	---	1200	25	---
21	51	7	---	1600	32	14
12	51	<10	---	2100	32	22

Visual examination of the surfaces of ingots from melt nos. 38 through 43 showed them to be less porous than those melted previously. Sectioning of several ingots at 25-mm intervals revealed no evidence of subsurface porosity. There was also no evidence of arc strikes to the 51-mm-diam (2-in.) copper mold, although arc strikes had always been observed for melts made in an argon atmosphere with this mold size. The skull formed on the top of the ingots (presumably by splatter and possibly, in part, by evaporation and condensation) was about 45 mm high for these melts and for melt no. 12. The skull was about 25 mm for melt no. 21, an ingot that was melted at a higher pressure and showed evidence of oxidation of the splatter. As the melting proceeded, the skull, which was on the order of 3 mm thick, was partially remelted into the ingot. In the case of melt no. 21, it appeared that the oxide on the splatter particles interfered with their remelting, creating a

porous surface and extensive subsurface porosity. The stainless steel skull apparently absorbs the energy delivered by any arc strike to the mold wall; it prevents damage to the mold, even in the case of the 51-mm-diam molds, which have always been damaged when used with argon backfill. The effect of mold condition (i.e., used mold vs wire-brushed or remachined mold) was also varied for melt nos. 38 through 43, with no observable effect on ingot appearance or in the appearance of sawed cross-sections.

Visual observation during the melt and the rounded appearance of the electrode stubs indicate a relatively large arc gap for these six vacuum melts. This is particularly true for the melt performed in the 51-mm mold at 2300 A (melt no. 39), for which the controller would not advance with sufficient speed to maintain a constant arc length. The current and voltage recordings show evidence of shorting of the electrode to the melt pool during portions of melts nos. 41, 42, and 43. As an example, the plots of current, voltage, and electrode position as a function of time (0.5-s increments) are shown in Fig. 2 for melt no. 41. Except during the time from about 75 s to about 130 s from the beginning of the melt, the current and voltage are very stable. This can be contrasted with a similar plot for a typical melt of stainless steel in an argon atmosphere shown in Fig. 3.

ORNL-DWG 89-19330

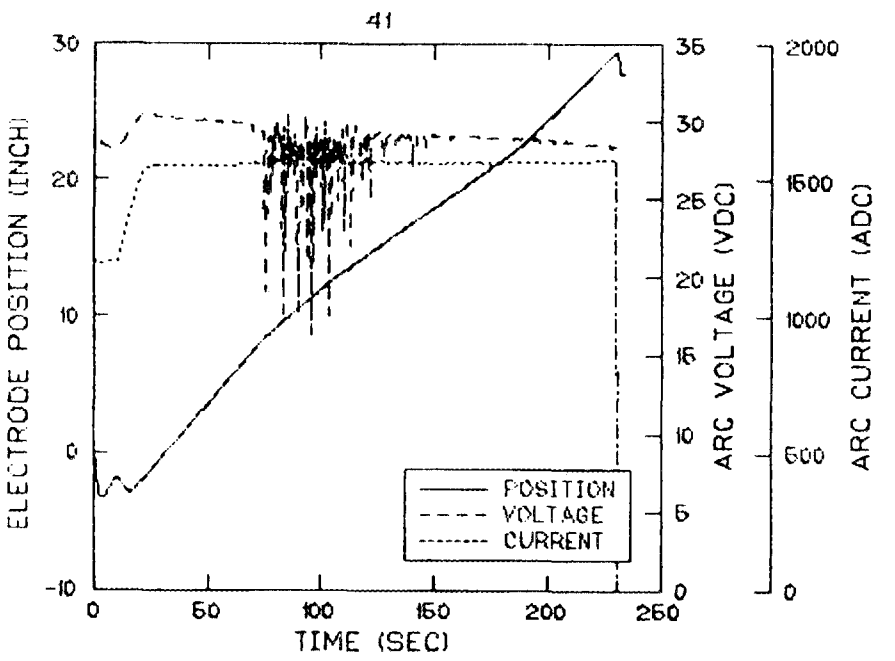

Fig. 2. Plot of melting parameters for arc melting of stainless steel in a 51-mm-diam mold in vacuum (melt 41).

ORNL-DWG 89-19331

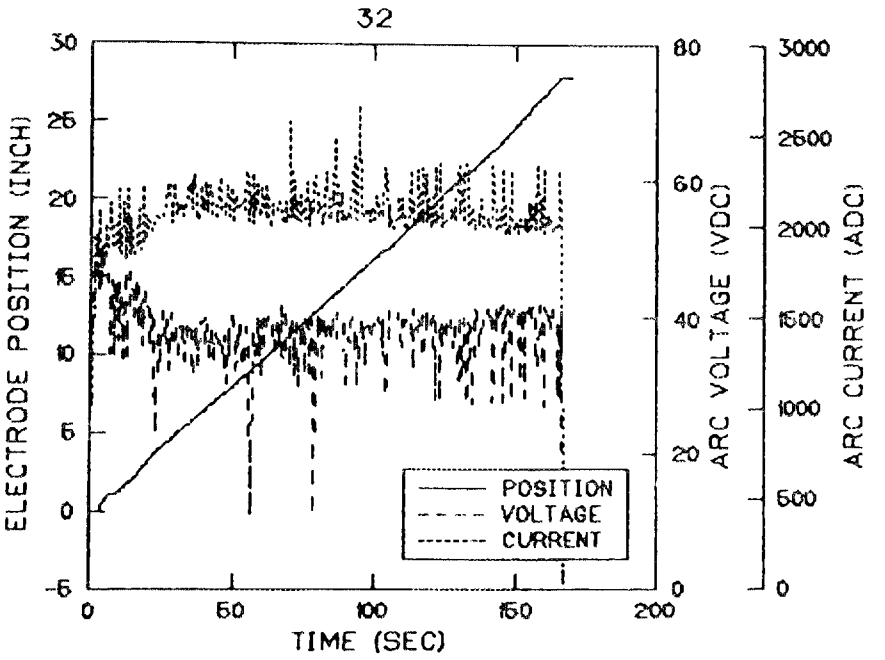

Fig. 3. Plot of melting parameters for arc melting of stainless steel in a 51-mm-diam mold using argon backfill (melt 32).

3.2 CONSUMABLE ARC MELTING OF SCRAP IRIDIUM ALLOY INGOTS

3.2.1 Arc Melting of the RS1 Electrode

A total of three consumable arc-melted ingots were made using scrap iridium alloy material in an effort to optimize the melting practice. The electrodes used and the resulting ingots were designated as RS1, RS2, and RS3. The RS1 electrode was fabricated by EB welding of 25-mm-diam drop-cast segments. The drop-cast segments were button melted using acid-cleaned solid scrap material that was being held for refining. The electrode was arc melted into a new 51-mm-diam crucible at an argon pressure of 68 kPa. The current was held between 2900 to 3200 A for the first half of the melt and 2300 to 2600 A for the second half of the melt to determine effects of current on ingot quality. Hot topping was completed at 2000 to 2100 A. The melting rate for the electrode decreased from 33 to 28 g/s as the current decreased. The total melting time was 240 s. A plot of the arc current, arc voltage, and electrode position is shown in Fig. 4. As seen in Fig. 5, the surface of the ingot showed scattered surface defects similar to those observed on the stainless steel ingots melted at the

ORNL-DWG 89-19332

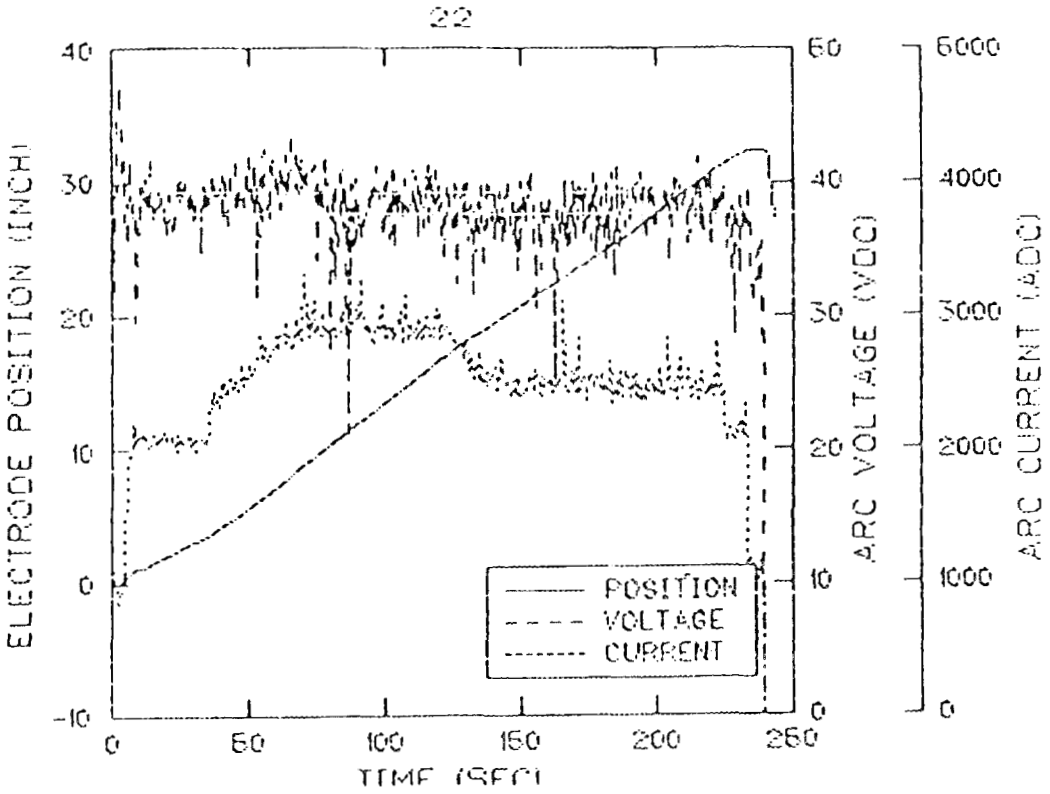

Fig. 4. Melt data plot for refinable scrap DOP-26 melt, RS1.

same pressure. The defects, which penetrate into the crucible, suggest that the arc struck the crucible wall with sufficient energy to cause wall damage but was not established for a long period. Control of the arc was maintained throughout the melt, and uncontrolled corona was not observed. The final ingot weight was 8.655 kg. The skull of the splattered material at the top of the ingot ranged from 13 to 19 mm high.

The RS1 ingot was cut to a 159-mm length and surface-ground before NDE. The diameter of the cast ingot varied from 49.6 mm at the bottom to 50.5 mm at the top, owing the taper of the mold. The ingot was ground to a 48.6-mm diameter, resulting in a 5% reduction in weight. Ultrasonic inspection, performed with wave propagation in both normal to ingot surface (radial) and at a 45° angle to the surface, indicated one subsurface defect, predicted to be a small pore approximately 0.8 mm below the surface. Since all surface defects had not been removed in grinding, these defective areas could not be determined to be free of subsurface defects. An additional 0.8 mm was removed from the ingot diameter by grinding, resulting in an additional 3% reduction of ingot weight. Reinspection by ultrasonic

YP-4858

Fig. 5. Cast RS1 ingot and electrode stub shows evidence of intermittent arcing to mold wall.

testing revealed the previously identified defect, now closer to the surface, but indicated no new defects.

Following ultrasonic inspection, the RS1 ingot was extruded to a round bar for subsequent remelting. The 47.9-mm-diam iridium ingot was cleaned with solvents and placed in a

molybdenum can of 75-mm OD. The can was heated to 1325°C and extruded through a 37.5-mm-diam die opening. The breakthrough load for the extrusion was 5.7 MN, corresponding to an extrusion constant of 835 MPa. The molybdenum was removed by pickling in an aqueous solution of 50% nitric acid with subsequent additions of sulfuric acid (about 5%). The cleaned bar of 25.1 mm diameter and 580 mm length showed a mass loss of 10 g of iridium, as measured for both extrusion and molybdenum pickling. A portion of the bar, 380 mm long from the tail end, was used for additional melting experiments with the RS2 electrode. A 150-mm-long section taken from the nose end was used for fabrication of a new electrode stub in order to improve alignment during EB welding of subsequent electrodes. The remaining 78-mm-long section, corresponding to the portion of the ingot containing the subsurface flaw indication, was processed to 51-mm-diam blanks, the aim of this being to determine a relationship between ultrasonic indications of flaws in the ground ingot with those subsequently found in finished blanks.

The processing of the RS1 extrusion section followed the same practice as used for processing of all extruded bars, except that the 25-mm-diam round bar was first press-forged between molybdenum covers to a rectangular cross-section 12.7 mm thick by 38 mm wide, using a 1200°C preheat temperature. The ultrasonic inspection of the eight blanks produced from this bar indicated a flaw in one blank, the first as measured from the nose end. This is approximately where the defect detected in the ingot was expected to be. However, the uncertainties in the material flow during extrusion and in maintaining the rotational orientation of the round extrusion to the ingot are such that a one-to-one correlation of the ultrasonic indications cannot be made with any certainty.

3.2.2 Arc Melting of the RS2 Electrode

The RS2 electrode was fabricated from the 380-mm length of the RS1 extrusion and 5.2 kg of additional scrap in the form of 25-mm-diam drop castings. The melting was performed in a remachined 54-mm-diam copper mold. The purpose of the melting experiment was to determine if a decrease in the vacuum pressure before and during melting of an iridium alloy would inhibit the arcing to the mold wall in a similar manner as had been observed with the melting of stainless steel. An initial vacuum level of 1.2 mPa was obtained for this melt. The vacuum chamber pressure varied between 7 and 13 mPa during the actual melting period. The arc current, arc voltage, and electrode position measurements are shown in Fig. 6. The arc current and voltage plots show more variation and evidence of short-circuit events than seen for other melts of either stainless steel or iridium. The arc current

ORNL-DWG 89-19333

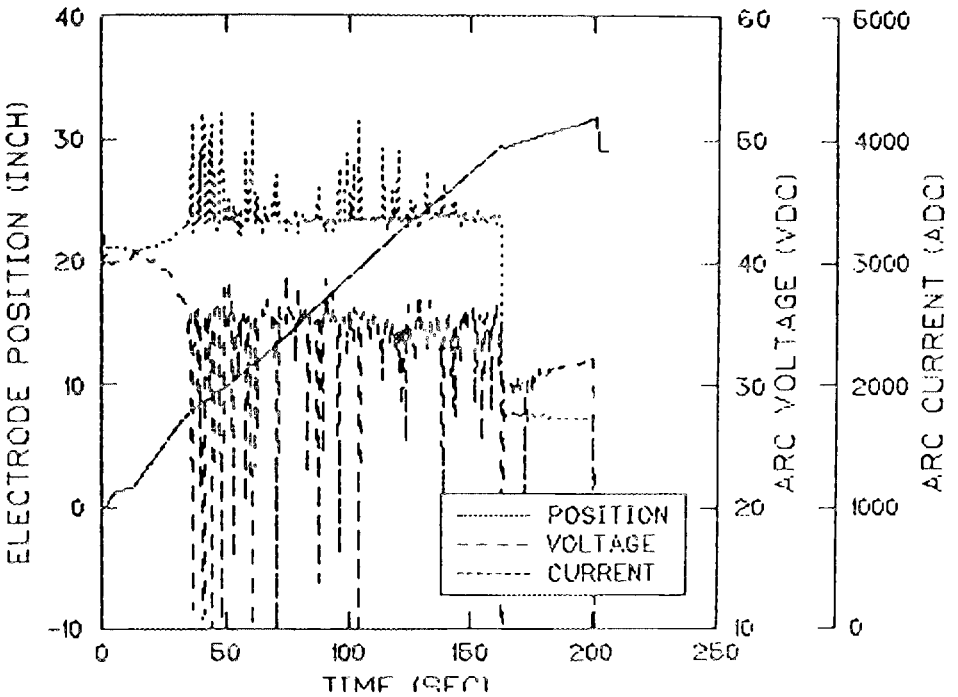

Fig. 6. Plot of arc current, arc voltage, and electrode position for RS2 iridium alloy refinable-scrap ingot melted in a 54-mm-diam mold.

averaged approximately 3400 A and the arc voltage approximately 33 V. The electrode feed rate was 33 g/s.

The surface condition of the vacuum-melted RS2 ingot, as shown in Fig. 7, exhibits surface defects similar to those obtained for the RS1 ingot melted with an argon backfill. The degree of damage to the copper mold was also similar to that for RS1. The surface condition of the iridium alloy ingot arc melted in vacuum was similar to that of the ingot melted in argon. This result differs from that obtained with stainless steel simulation melts in the same 51- to 54-mm-diam range.

3.2.3 Arc Melting of the RS3 Electrode

The RS3 refinable-scrap electrode was produced by extrusion of the previously melted RS2 ingot. The ingot was canned in molybdenum and extruded through a 37.5-mm-diam die opening and straightened on a forge press. After the molybdenum was desolved in an acid

Fig. 7. DOP-26 iridium alloy refinable-scrap arc-melted ingot (54-mm diam). Front view of RS2 ingot.

bath, an iridium alloy bar approximately 28 mm in diameter and 600 mm long was obtained and used to fabricate an electrode designated RS3.

In preparation for melting, the electrode was aligned with respect to the mold flange as well as possible. The calculated electrode-to-mold gap varied from 16 to 21 mm. A new

mold 63 mm ID by 12.7 mm wall thickness was cleaned and placed in the melting chamber. A 51-mm-diam iridium alloy pad was placed in the mold with additional DOP-26 alloy scrap chips and pieces to fill the gap between the pad and mold. The furnace was pumped to a vacuum of 1.5 mPa, the arc struck to the pad, and the electrode melted at an arc current of 3500 A. Cooling water flow was 0.0019 m^3/s. The pressure in the chamber was generally in the range of 13 to 17 mPa during the melt. At the end of the melt, the current was dropped to 1800 A for hot topping of the ingot.

The surface of the RS3 ingot, shown in Fig. 8, is quite smooth overall, but a number of locations exhibit surface porosity. The overall surface appearance is much better than that of the RS2 ingot, melted in a 54-mm-diam mold and shown in Fig. 7. Examination of these regions of surface porosity invariably reveals smooth, shiny surfaces near the bottom of the pores, usually with a rippled appearance. The ripples appear to be melted lines associated with a nonuniform rate of solidification of the molten surface. An example of this is shown in Fig. 9. Similar ripples in the top surface of the ingot are clearly due to variations in the solidification rate caused by small variations in arc power. Because of the protuberances on the surface of the ingot, some pressure was required to remove it from the mold, and some damage to the mold was also observed. Nevertheless, the damage was significantly less than that of the 54-mm-diam mold for the RS2 ingot. The arc current, arc voltage, and relative electrode position for the RS3 melt are shown graphically in Fig. 10. The large variations in arc current and voltage during the time between 20 and 60 s from the start of the melt are believed to be brief periods of short- circuiting of the electrode to the molten pool due to a small arc gap. The remainder of the melt shows relatively little variation in arc current and voltage. By contrast, the arc current and voltage for the RS2 ingot exhibit numerous short-circuit events after 40 s and for the entire remainder of the melt (Fig. 6). We do not know whether the arc shorts to the molten pool or to the mold wall. A comparison of the relative degree of surface porosity on various portions of the RS3 ingot with the calculated electrode-to-mold arc gap during solidification of that portion of the ingot does not show any consistent relationship between the two. Neither is there a correlation between the regions of surface porosity, which are more or less randomly distributed over the entire length of the ingot, and the occurrence of short-circuit events during melting as monitored by arc current and voltage.

YP-6182

Fig. 8. DOP-26 iridium alloy refinable-scrap arc-melted ingot (63-mm diam). Front view of RS3 ingot.

Fig. 9. Pore on the surface of arc-melted RS3 iridium alloy ingot. A generally smooth melted surface is seen at the base of the pore with ripples on the melted surface. These are associated with a nonuniform solidification rate. Magnification: 16X.

ORNL-DWG 89-19334

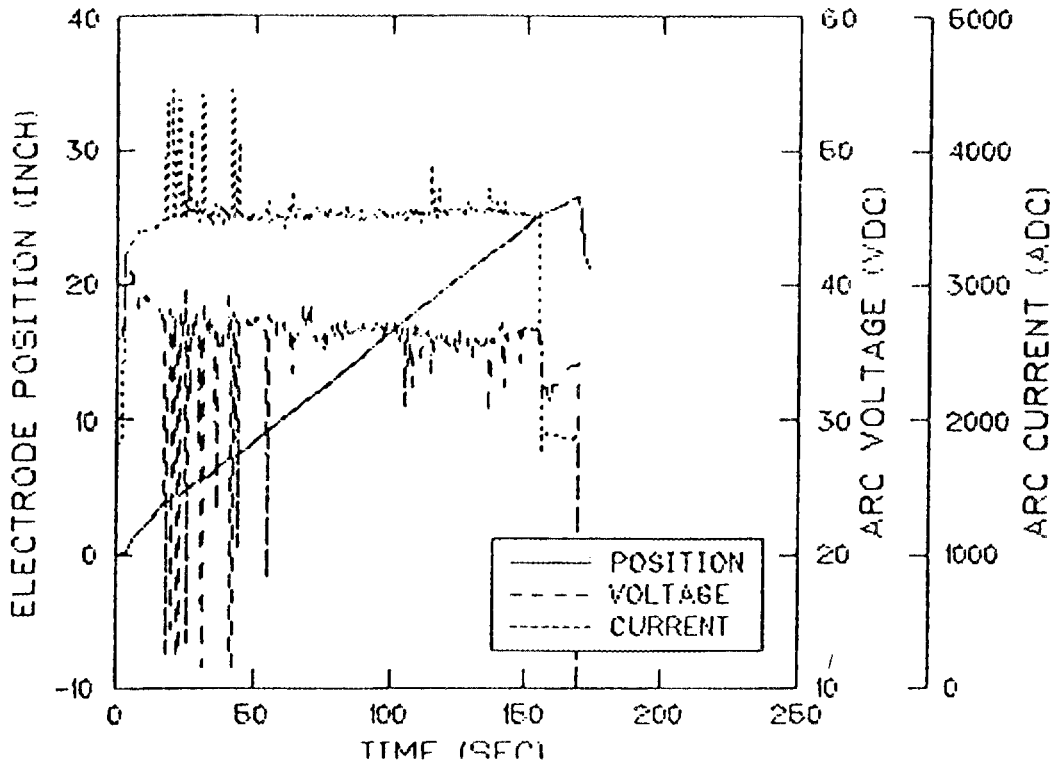

Fig. 10. Plot of arc current, arc voltage, and electrode position for RS3 iridium alloy refinable-scrap ingot melted in a 63-mm-diam mold.

4. PROCESSING OF IRIDIUM ALLOY INGOTS

4.1 PROCESSING OF BR6 BLANKS

The BR6 ingot was fabricated from recyclable material (B and XR ingots) and processed to blanks during 1987. Ultrasonic indications were found on all nine sheets fabricated from this ingot, and small blisters were observed on several sheets. Material from sheets 1 and 2, corresponding to a total of 12 blanks, was not processed as a result of the ultrasonic inspection. The NDE of the blanks resulted in rejection of 21 of the 63 blanks inspected. The rejected blanks were all from sheets 1, 4, 5, 7, and 8, and occurred in sequences of three to five adjacent blanks.

4.2 PROCESSING OF C1 BLANKS

The C1 ingot had been processed to alloy sheet during FY 1987. The fabrication and evaluation of alloy blanks was completed during FY 1988. The 19.3-kg C batch of iridium powder was obtained through Westinghouse Materials Company of Ohio. The chemical analysis of the material showed it to be within specification. Ten kilograms of Ir-0.3 wt % W powder compacts were EB melted, alloyed, and fabricated into the C1 electrode. The electrode was arc melted to produce a 7.67-kg ingot 51 mm in diameter, which was canned and extruded to rectangular bar using a 1300°C preheat temperature with a reduction ratio of 6.5:1. The total transfer and extrusion time was 25 s. The extruded bar was cut into eight sections for hot rolling, the sections being numbered sequentially as C1-1 through C1-8, starting at the nose end of the extrusion. The extruded sections were covered with a 1.5-mm-thick molybdenum sheet and then cross-rolled from a thickness of 11.7 to 4.5 mm in five roll passes of 20% each with 20-min preheats and reheats at 1200°C. The rolled plates were acid cleaned and recrystallized at 1300°C for 1 h in vacuum at a pressure of 1.1 mPa (8×10^{-6} torr). All subsequent rolling with molybdenum covers was performed at 1100°C using reductions of 20% or less per pass. Rolling of the sheets at 900°C was performed only to obtain uniform sheet thickness. Following recrystallization one probable delamination defect was observed at one end of one plate during examination of the cut ends at 30× magnification. Blisters observed on one side of the C1-4 through C1-7 plates and on both ends of C1-8 were removed by grinding with tungsten carbide burrs, a process similar to that used on standard process arc-cast ingots, prior to continued sheet rolling. Ultrasonic inspection showed all sheets to contain indications of near-surface defects. Blanks were cut and ground in order to determine if the defects were located in the surface and would be removed in grinding.

A metallographic section through one of the blisters shown in Fig. 11 indicates that the blister is caused by a subsurface delamination containing a high vapor pressure contaminant which caused swelling during vacuum recrystallization. The subsurface defects are believed to be the result of the melted covering unremelted splatter below the surface of the consumable arc-cast ingot.

The sheets in which blisters were found after recrystallization were found to have high rejection rates on NDE. The distribution of blisters and NDE results are summarized in Table 6. Sheets C1-1 and C1-2 showed no evidence of blisters and yielded 12 of 16 blanks in the initial inspection and 3 additional acceptable blanks following rework. Three acceptable blanks were obtained from the four possible blanks that were electrodischarge-machined

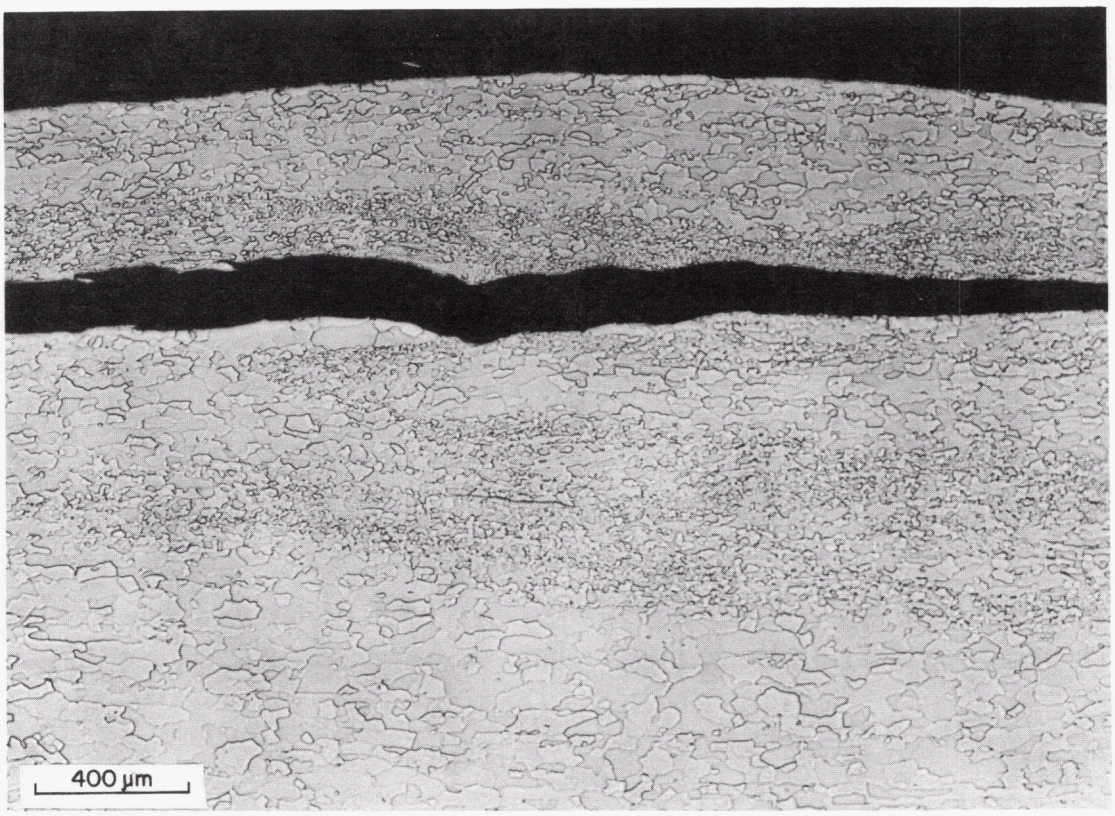

Fig. 11. Cross section through a blister in sheet C1-7 following recrystallization at 1300°C shows a large subsurface defect.

Table 6. Distribution of blisters in recrystallized sheets and rejected blanks from C1 ingot

Sheet	Possible blanks	Blisters			Nondestructive examination rejections			Accepted blanks (including rework)
		Side A	Side B	Total	Visual	Penetrant	Ultrasonic	
1	8	0	0	0	0	2	0	7
2	8	0	0	0	1	1	0	8
3	4	3	0	3	0	2	0	3
4	8	2	1	3	0	3	5	0
5	7	7	0	7	0	1	6	0
6	8	13	0	13	0	0	8	0
7	7	9	0	9	0	0	7	0
8	7	5	8	13	0	0	7	0

from sheet C1-3, which had showed evidence of blistering. The incidence of blistering increased in sheets C1-4 through sheets C1-8 resulting in rejection of all blanks. Further, only one of the six reworked blanks that passed ultrasonic inspection could pass subsequent penetrant inspection. This behavior is in contrast to that of blanks from sheets C1-1 through C1-3 and to blanks from previous ingots, for which the large majority of reworked blanks with only surface defects were ultimately acceptable.

Tensile impact tests were performed on samples of C1 material corresponding approximately to nose, center, and tail locations on the extrusion. The tensile elongations at 980°C and an impact velocity of 61 m/s of specimens recrystallized 19 h at 1500°C all exceeded the minimum required value at 13.5%. The elongation values were 17.4% for the nose, 16.0% for the center, and 14.2% and 23.2% for tail samples. The chemical analysis, the metallographic analysis, and the hardness test results for C1 were all within specification. These results qualify the C-batch powder for production. The variability in the yield of acceptable blanks from sheet to sheet could not be associated with any systematic variation in chemical analysis within the specification limits and may be attributed to arc-melting defects.

4.3 PROCESSING OF D1 INGOTS

4.3.1 D1 Electrode Preparation

Approximately 20.1 kg of iridium powder (designated D batch) were received from Engelhard Corporation. During the weighing of the powder for receiving inspection, four out of five jars were noted to contain several lumps of agglomerated powder up to 6.35 mm (0.250 in.) in diameter. These agglomerates are out of specification, as all powder is to pass through a 150-μm screen (U.S. sieve size 100). Analysis of the powder without agglomerates by the spark source mass spectroscopy (SSMS) method showed the composition to be within specification. Samples of the agglomerates analyzed by SSMS separately showed that they are also within specification. Results from quantitative screening averaged 4.1 wt % of the powder in excess of U.S. sieve size 100. Based on these results, the powder was accepted for fabrication of flight-quality hardware. The screened powder was made into master blends, water washed, blended with tungsten to produce the Ir-0.3 wt % W mixture, and compacted. A total of 12.6 kg of compacts were sintered and EB melted. Arc-melted buttons were alloyed with thorium and aluminum master alloys and drop cast into 25-mm-diam electrode segments. The segments and the threaded stub were EB welded to produce the D1 electrode, weighing 11.4 kg.

4.3.2 D1 Arc Melting and Ingot Preparation

The D1 electrode was installed in the arc-melting furnace and aligned by raising and lowering the actuator several times to assure reproducibility. The maximum deviations from concentricity measured in the down, mid-length, and up electrode positions were 0.7, 0.5, and 3.5 mm, respectively. This corresponds to minimum electrode-to-mold clearances of 12, 12, and 9 mm at the top, middle, and bottom, respectively, of the ingot. The electrode was then melted into a new 51-mm-diam mold at a pressure of 68 kPa (0.66 atm argon). The vacuum pressure prior to backfilling was 4 mPa; the arc current was between 2500 and 2700 A; the average voltage was 38 V; and the melting time was 4.5 min, which gave an average melting rate of 30 g/s. The arc current, arc voltage, and electrode position are shown graphically in Fig. 12.

ORNL-DWG 89-19335

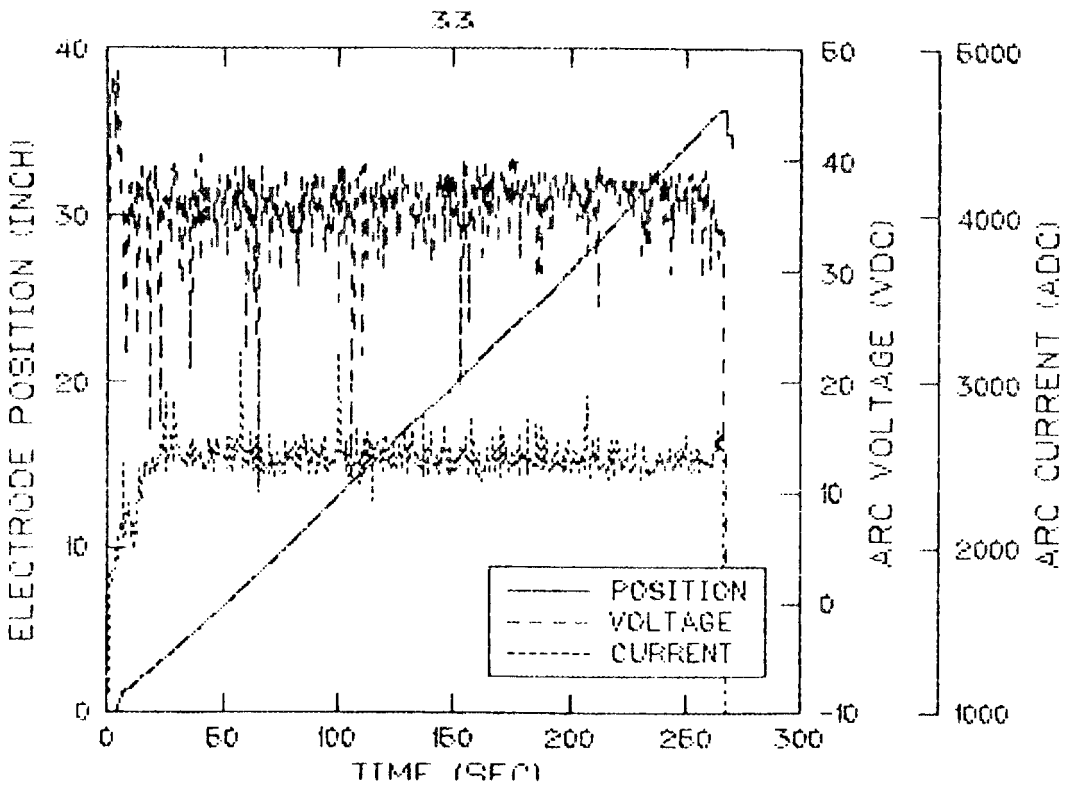

Fig. 12. Plot of arc current, arc voltage, and electrode position during arc melting of D1 iridium alloy electrode.

The surface of the ingot was generally bright with scattered surface defects, as seen in Fig. 13. Defects were also noted in the copper mold. Their appearance suggested that the arc had struck the mold wall. Although the D1 ingot was melted under conditions similar to the RS1 ingot, more surface defects attributed to arcing occurred, and unfused splatter was observed on the as-cast surface. The unfused splatter was attributed to holding a shorter arc. The shorter arc length, which was associated with the lower arc voltage as compared to the RS1 ingot, decreased the size of the molten pool. The shorter arc length was used in an effort to minimize arcing to the copper mold but did not appear to have been effective. The splatter ring at the top of the ingot ranged from 13 to 19 mm.

The ingot was ground from an initial diameter of 49.9 mm to a diameter of 47.0 mm using a resin-bonded 100-μm diamond wheel with a feed of 0.013 mm per pass. The ingot was cut, and the ends were ground with an alumina wheel to a finished length of 162.2 mm.

Nondestructive examination of the ingot included examination by a low-power binocular microscope, dye-penetrant testing, and ultrasonic inspection. There were many surface defects apparent on the ground D1 ingot. Visual examination in the binocular microscope showed many of these surface defects to be annular in shape, indicating that they are caused by unremelted splatter. Dye-penetrant inspection revealed the presence of a crack on the top surface extending about 19 mm from the circumference of the ground ingot and about 13 mm from the top of the ingot, as seen in Fig. 14. Ultrasonic inspection was performed using pulse propagation in directions of both normal to and angled at 45° with respect to a tangent to the circumferential surface. Four ultrasonic indications at a depth greater than 0.8 mm were obtained with the angled pulse, and one indication at a depth of about 5 mm was obtained with the normal pulse. No further surface grinding was performed on this ingot in order to avoid excessive loss of material.

4.3.3 D1 Extrusion and Rolling

The ground D1 ingot was cleaned and placed in a molybdenum can similar to those used previously. The tail plug for the can was modified to increase the thickness from 13 to 25 mm and the material changed from molybdenum to the higher-strength TZM molybdenum alloy. The modification was intended to minimize the suck-in at the tail of the extrusion and increase the usable length of iridium alloy bar. A notch was made on the flat portion of the front of the can to reveal orientation after extrusion. The ingot was oriented such that two of the ultrasonic indications of defects were within 7° of the die opening width direction, which

YP-5459

Fig. 13. Arc-melted D1 iridium alloy ingot and electrode stub.

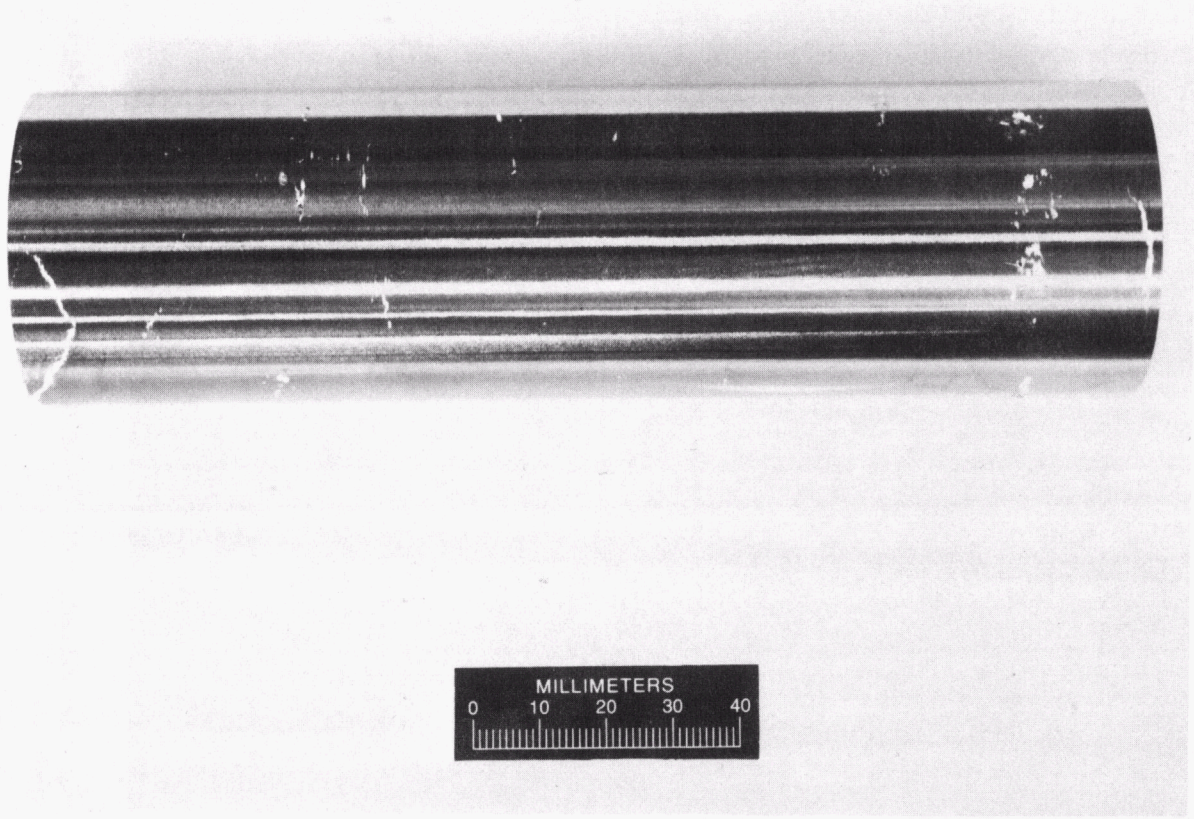

Fig. 14. Iridium alloy ingot D1 following surface grinding and dye-penetrant inspection.

would be expected to result in their location at the outer edge of the rolled sheet. One indication was within 5 mm of the tail end. The fourth indication, located 13 cm from the nose end of the 16-cm-long ingot, was of necessity oriented 16° from the die opening height direction, which would be expected to result in its location near the centerline of the rolled sheet.

The canned D1 ingot was preheated for 4 h at 1325°C and extruded in 76-mm-diam tooling through a rectangular die opening of 19 by 38 mm. The maximum extrusion load was 6.25 MN (or 93% of the press capacity), corresponding to an extrusion constant of 700 MPa. Total transfer time from the furnace to extrusion was 15 s. On exiting the die, the extrusion caused both the die and the die-backer tooling to rotate about 30 to 40°. This created a twist in the extrusion. Although the twist did not interfere with subsequent processing, it did introduce considerable uncertainty in relating the rotational position of ultrasonic indications of defects in the ingot to specific locations on the extruded bar. The extruded bar was immediately straightened on the forge press and cooled in air to room temperature.

The new extruded bar was removed by pickling in an aqueous solution of 50% by volume of nitric acid with subsequent additions of sulfuric acid, up to a total of about 5%. This procedure maintains a reasonable dissolution rate of molybdenum without acid splatter. The cleaned iridium alloy bar was approximately 28 mm wide by 12.5 mm thick. Approximately 100 g of material was cut from the tail of the extrusion to remove the suck-in region and reach sound material. This was estimated to be between one-half and one-third of the material, which was required to be removed from extrusions that used the previous design of the plug on the molybdenum can. Visual examination of the tail revealed no evidence of cracks associated with the large dye-penetrant-revealed crack seen in the ground ingot.

Samples were cut from the extruded D1 bar at nose, center, and tail locations. Metallographic analysis of the material extruded at 1325°C showed the material to be about 50% recrystallized. The microstructure was uniform over the length of the bar, as can be seen in Figs. 15, 16, and 17. This can be contrasted with the microstructure shown in Fig. 18, of the B2 bar extruded at 1250°C, which was fully recrystallized. The B2 extrusion also exhibits more prominent etchant attack of the coarse, elongated cast grain boundaries. The differences in the microstructure are not easily explained, since the higher extrusion temperature would normally be expected to result in a greater amount of recrystallization. Chemical analysis of samples from the D1 extruded bar by SSMS showed the material to be within specification.

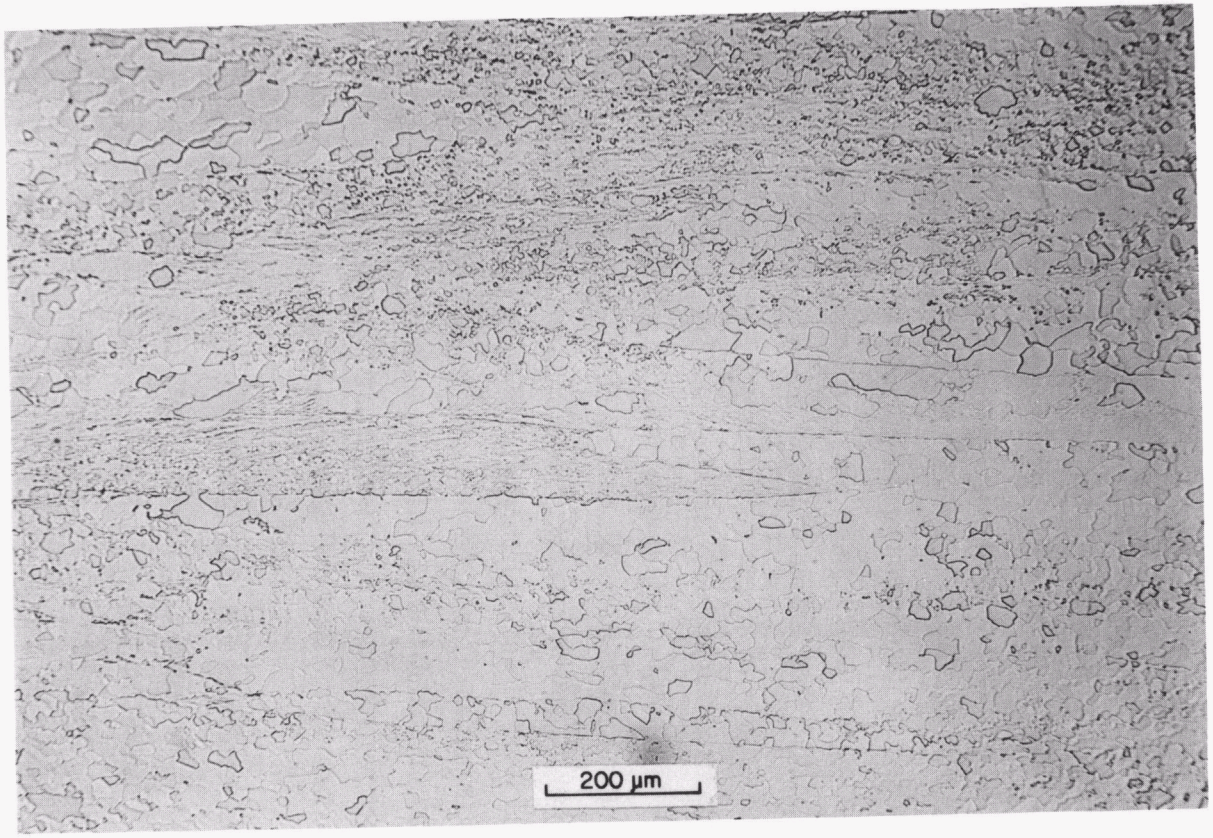

Fig. 15. Microstructure of D1 bar extruded at 1325°C. Longitudinal section from nose portion of bar.

Y211333

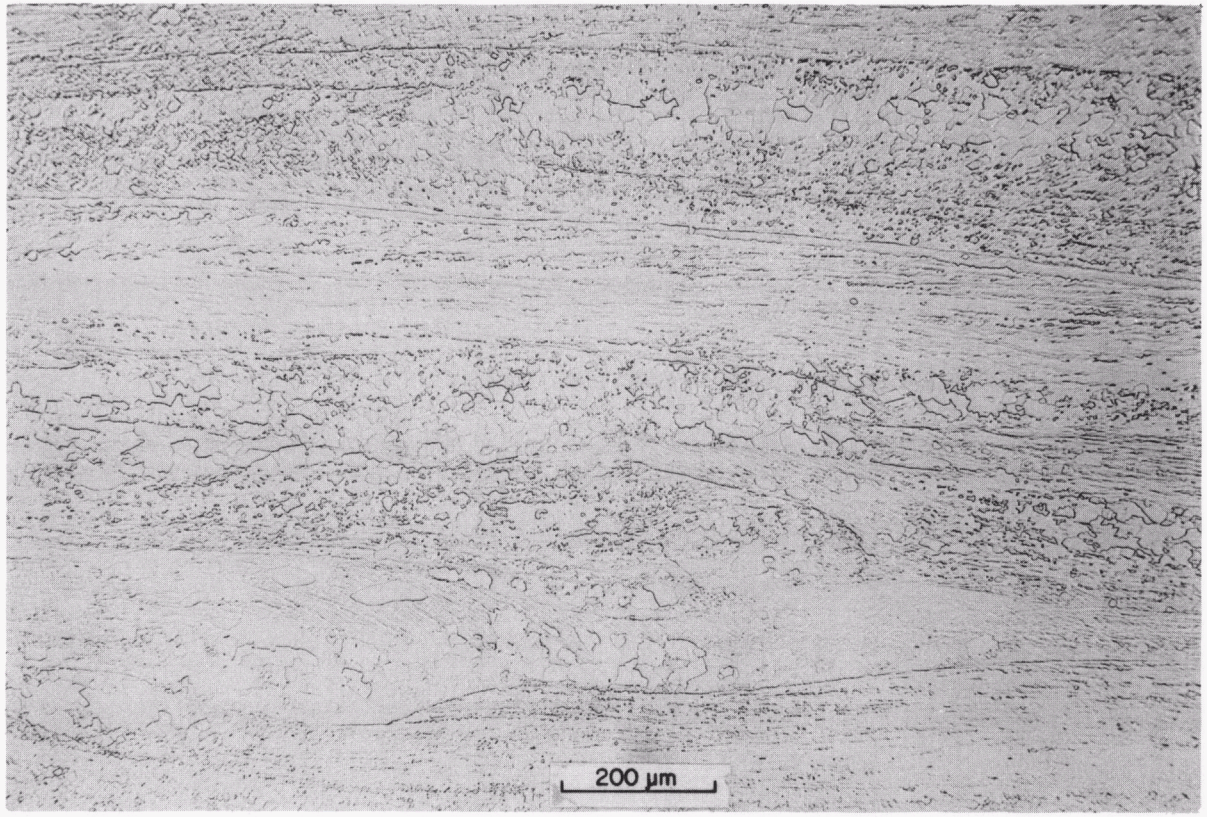

Fig. 16. Microstructure of D1 bar extruded at 1325°C. Longitudinal section from center portion of bar.

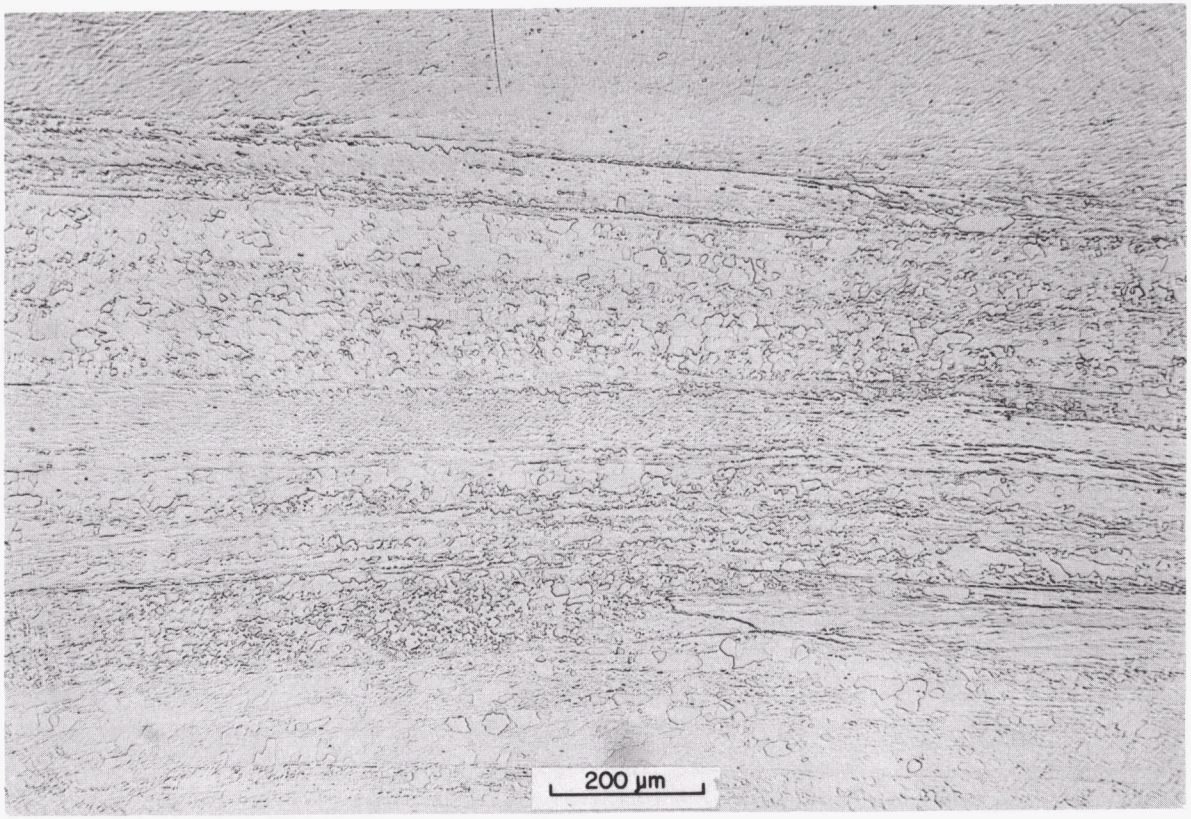

Fig. 17. Microstructure of D1 bar extruded at 1325°C. Longitudinal section from tail portion of bar.

The iridium alloy bar was cut into ten rolling billets, each approximately 89 mm long. Seven of the ten billets (D1-1, D1-4, D1-5, and D1-7 through D1-10) were cross- rolled using standard procedures and recrystallized at 1300°C for 1 h in vacuum. Visual examination of rolled surfaces at a magnification of 10× showed no indication of blisters, as were found previously on the C1 material. The rolling of these materials was continued using standard procedures.

4.3.4 D1 Blank Inspection

The seven rolling billets from the D1 extrusion, which were rolled to sheet, produced 49 blanks, one of which was rejected at dimensional inspection because of an error in the blanking procedure. The NDE of remaining blanks is summarized in Table 7. Ultrasonic indications of defects were detected in the last blank from sheet 7, in four of seven blanks

Table 7. Result of ultrasonic inspection of blanks from D1 ingot

Identity of sheets	Number of blanks		Identity of rejected blanks
	Inspected	Rejected	
1	6	0	
4	7	0	
5	7	0	
7	7	1	7
8	7	4	2, 4, 6, 7
9	7	5	1, 2, 3, 4, 5
10	7	1	5
Total	48	11	

from sheet 8, and in the first five blanks from sheet 9. If the extrusion process is approximated as an ideal deformation with no redundant deformation, the one ultrasonic indication from the ground ingot, which was not oriented during extrusion so as to be near the edge of the rolled sheet, would be expected to appear in the first and second blanks from the ninth sheet. The other three indications from the ground D1 ingot would correspond to the third blank of the second sheet, the second and third blank of the eighth sheet, and the fifth blank

Y202540

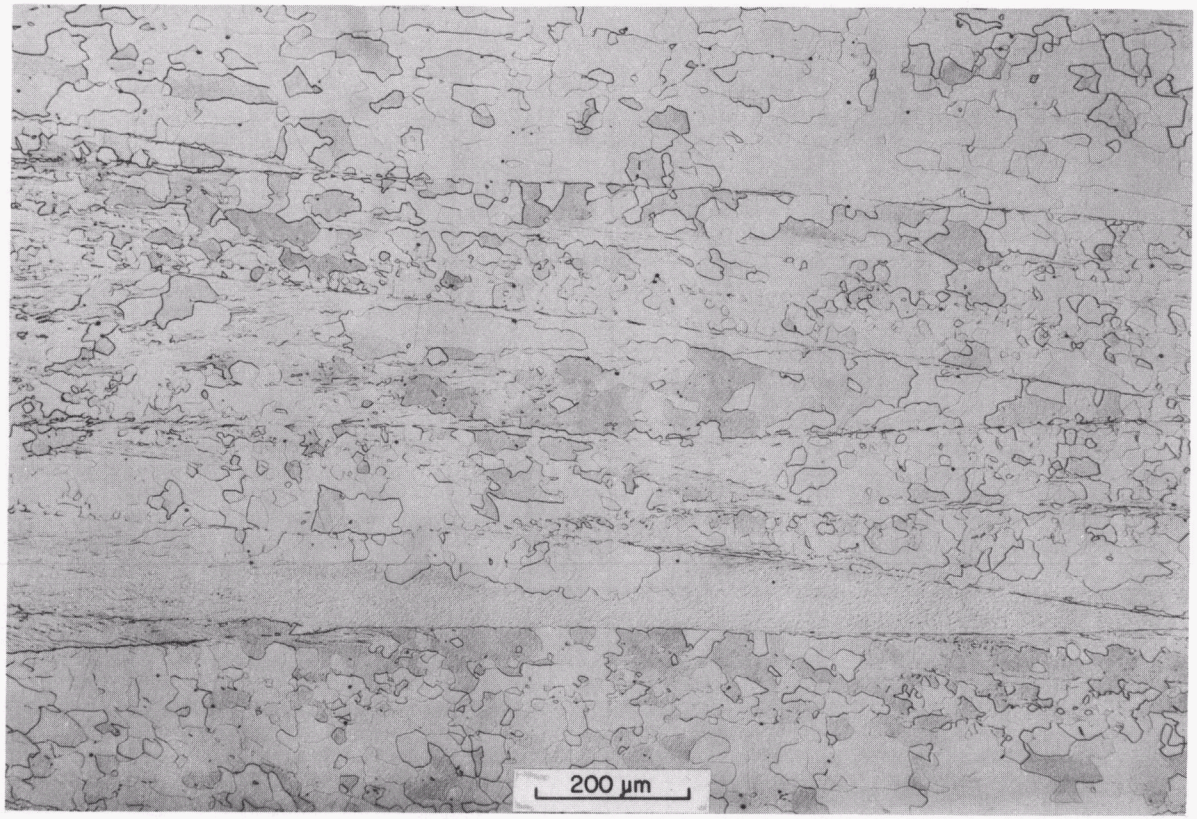

Fig. 18. Microstructure of B2 bar extruded at 1250°C. Longitudinal section from tail portion of bar.

1/29 of the material from each jar was removed and placed in one of the other jars. Each of these jars was then blended to make a batch blend.

The material for the E1 electrode was prepared from four batch blends. No powder washing was performed. Originally, the powder-washing step was incorporated in order to purify incoming powder that was contaminated with water-soluble salts, as was typical in the early 1970s. The current powder does not contain these water-soluble impurities in any significant amount. In addition, the EB melting process is very effective in removing these high vapor pressure impurities if present. Compacts of the Ir-0.3 wt % W were prepared from the batch blends and pressed at a load of 400 kN. The applied load was decreased from the 800 kN used previously in order to obtain better outgassing during sintering, which would result in lower splatter losses during EB melting. The lower compaction pressure also permitted the use of the lower capacity press in the same building as the powder blending facilities. The behavior of the powder compacts during hydrogen outgassing and vacuum sintering was similar to that of compacts pressed at the higher load.

A total of 12.1 kg of compacts for E1 electrode was melted eight times. The initial weight and the weight after each melt are shown in Fig. 19. The weight loss of the

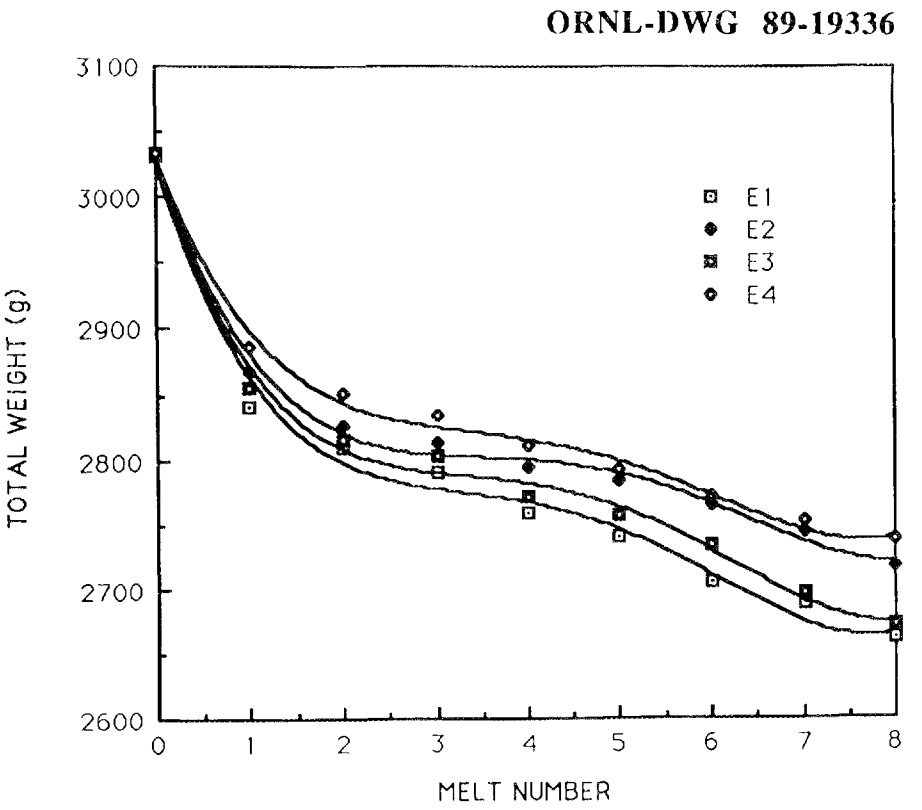

Fig. 19. Weight losses during electron beam melt refining of the four batch blends used for E1 electrode.

EB-melted buttons during the first of eight melts averaged 5.6% of the initial compact weight. The total weight loss for the entire EB melting process averaged 11.0%. The weight loss during the initial melting of the compacts was primarily the result of splatter from residual gas in the sintered compacts. The subsequent button weight losses were primarily the result of metal vaporization.

The EB-melted buttons were alloyed with master alloys of thorium and aluminum with iridium by nonconsumable button arc melting and then drop cast into a 25-mm-diam mold. Two individual alloy drops were sufficient to fill the mold and produce an electrode segment approximately 5 mm long. The E1 electrode was fabricated by EB butt welding of eight such segments. The cavity at the top of each electrode segment was filled by EB welding of pieces of E1 iridium alloy prior to butt welding in order to minimize porosity in the electrode. The soundness of the fabricated electrode was evaluated by electrical resistance measurements. Measurements were made of potential drops along 25-mm increments of length at a constant direct current of 11 A. An average of two measurements with forward polarity and two measurements with reverse polarity was obtained. The measurements are shown as conductance, which should be proportional to an average effective cross-sectional area of the electrode, and are plotted in Fig. 20 together with a schematic representation of the E1 electrode. The schematic shows the presence of EB weld regions around the entire circumference and length of the electrode and also the presence of obvious lines of lack of fusion between two alloy drops within the same electrode segment. The conductance is generally about 0.3 $(\mu\Omega)^{-1}$ along those 25-mm lengths of the electrode produced from a single button. The conductance is generally in the range of 0.2 to 0.25 $(\mu\Omega)^{-1}$ along those 25-mm lengths of electrode containing the butt welds between two segments. The minimum conductance values of about 0.1 to 0.15 $(\mu\Omega)^{-1}$ occur frequently along those 25-mm lengths of the electrode lacking fusion lines between the drops of a single drop-cast segment. Fusion lines are absent because the upper surface of the alloy did not remelt in the mold when it came into contact with the molten material from the second drop.

4.4.2 E1 Arc Melting and Ingot Preparation

On the basis of the good results obtained with the arc melting of the RS3 refinable-scrap electrode in the 63-mm-diam mold, the decision was made to melt the E1 ingot under vacuum in a 63-mm-diam mold. The straightness and alignment of the electrode was similar to that of RS3. The calculated electrode-to-mold clearance varied from 16 to 22 mm for the

ORNL-DWG 89-19337

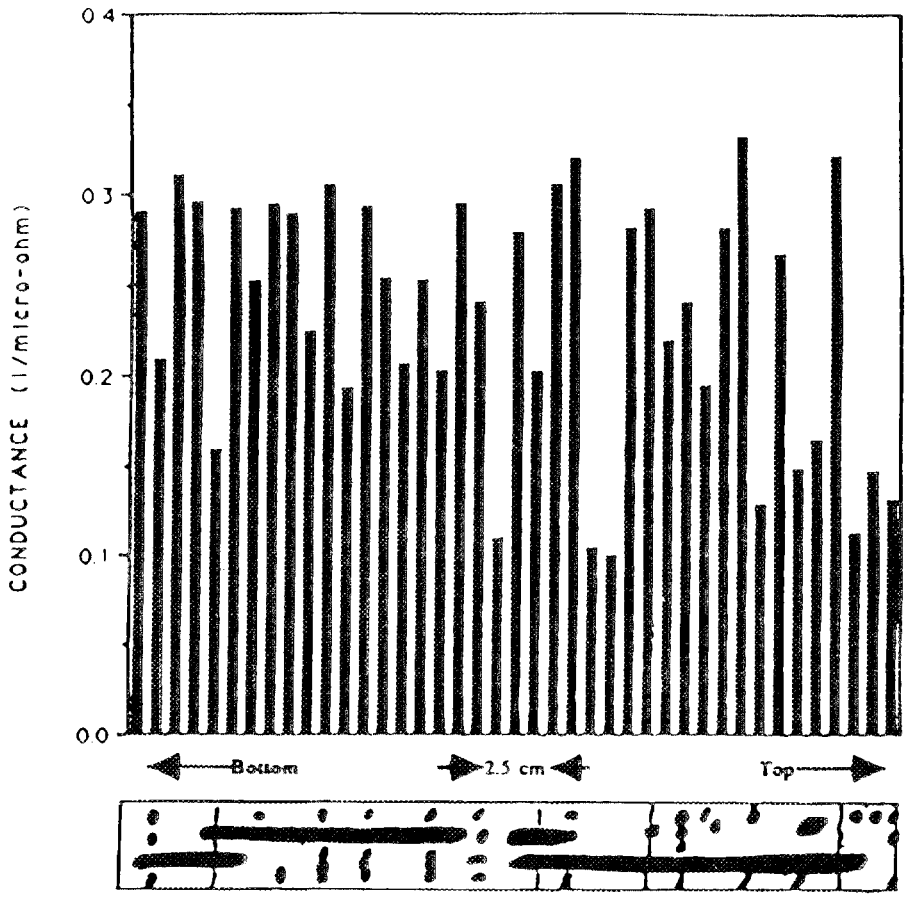

WELD
LACK OF FUSION LINE IN DROP CASTING

Fig. 20. Results on inspection of E1-welded electrode by electrical conductance measurements.

bottom of the ingot and from 18 to 21 mm for the middle and top of the ingot. The initial vacuum in the chamber was 1.5 mPa with a chamber vacuum during melting of 20 to 40 mPa. The arc current was between 3500 and 3600 A during the melt, with brief excursions to higher values during arc short-circuiting events.

The melting behavior deviated from that obtained for an earlier RS3 melt. That is, because of the limitations of the furnace, the feed rate for the electrode could not be maintained at a sufficiently high rate to maintain the arc gap. At approximately 100 s into the melt,

the operator could see that the arc gap was extremely large and manually fed the electrode to shorten the arc gap. The feed rate was then automatically controlled for the remainder of the melt. A total of 9890 g of alloy was melted. Figure 21 shows the arc current, voltage, and relative electrode position for melting E1. The higher voltage of the first 100 s corresponds to the larger than normal arc gap.

A photograph of the E1 ingot is shown in Fig. 22. The skull at the top of the ingot, consisting of unremelted splatter, is approximately 50 mm high, much higher than those seen on any previous iridium alloy ingot. The lower portion of the ingot also showed areas of partially unremelted splatter. This portion was melted with an unusually long arc gap. The upper portion of the ingot showed fewer regions of unremelted splatter, but there were some regions with a raised surface, which caused damage to the copper mold.

The results of arc melting of the E1 ingot into a 63-mm-diam mold were an improvement in surface appearance as compared to the ingots melted into a 51-mm-diam mold. The problem of controlling the arc gap between the electrode and the melt pool is a potential source of variability in ingot quality. A new arc-melting furnace is needed to achieve a reproducible gap between the electrode and the pool as well as to improve electrode alignment with respect to the mold wall.

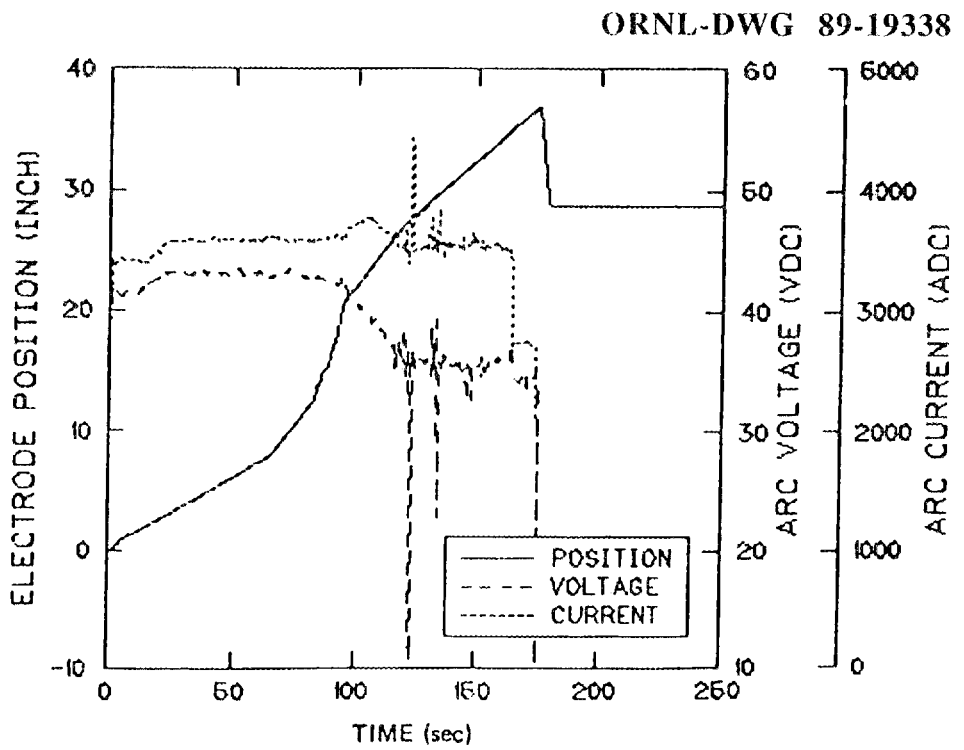

Fig. 21. Plot of arc current, arc voltage, and electrode position for E1 iridium alloy ingot melted in a 63-mm-diam mold.

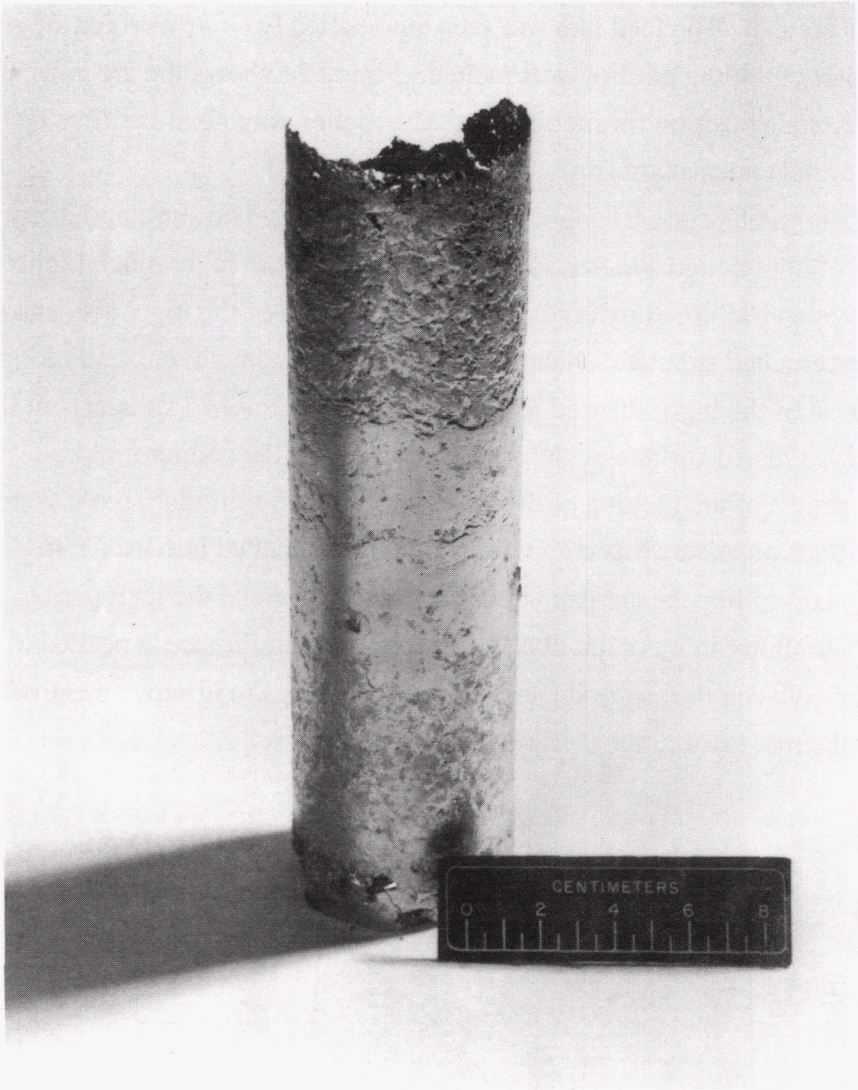

Fig. 22. E1 ingot vacuum arc melted in 63-mm-diam mold. The skull of unremelted splatter at top of the ingot is larger than other iridium ingots. The surface quality is considerably improved over the smaller diameter D1 ingot.

After the ingot was acid cleaned, the skull material was broken loose and used to fill the shrinkage cavity in the top of the ingot by EB welding, in a manner analogous to that used to fill the shrinkage cavity in the standard process rectangular drop castings. Although the EB welding left several small cracks in the weld metal, these cracks should not interfere with subsequent processing. This procedure avoids the necessity of cutting off the top of the ingot, which typically creates about 1 kg of recycled material, and is a particularly useful

technique for the larger 63-mm-diam ingots, which, owing to the limits on the electrode length, are substantially shorter than the 51-mm-diam ingots.

The pad at the bottom of the E1 ingot was cut off, and the ingot, which tapered from 62.3 mm in diameter at the bottom to 63.1 mm in diameter at the top, was then ground with a diamond wheel to a 61.5-mm diameter. A photograph of the ground ingot is shown in Fig. 23.

YP-6394

Fig. 23. E1 ingot, after grinding to 61.5-mm diam.

5. MATERIALS USAGE IN ALLOY BLANK PROCESSING

The generation of intermediate products, recycle material, and scrap for refining, as well as material loss, during the processing of D1 and E1 electrodes has been documented and is summarized here. The resulting material balances are the basis for estimates of materials distribution anticipated for future iridium blank production.

The materials balance for fabrication of the E1 electrode from powder compacts is shown in Table 8. The input consists of powder compacts and master alloy pieces. The

Table 8. Materials balance for E1 electrode fabrication

Type	Form	Weight (g)
	Input	
Virgin	Compacts and master alloy	12,184
Recycle	Electrode stub	768
	Total	12,952
	Output	
Virgin	Alloyed electrode	10,823
Recycle	Drop-casting skull	548
Residual	Electron beam melt scrap	1,340
Residual	Arc melting and cutting scrap	170
Loss	Electron beam welding loss	71
	Total	12,952

output consists of the alloyed electrode, skull material from the last drop casting in the series which produced the electrode segments, EB melting and arc melting residuals that are partially recovered as scrap, and material losses in EB welding of the electrode. Residual is defined as the book value of iridium removed in a process operation. The removed material may become mixed with other materials such as abrasives. The losses in the powder preparation are not included here but are known to be small. Significant amounts of out-of-specification oversize powder consisting of agglomerates of finer particles may be removed

during screening, but these have been used in the past, after acceptance of chemical analysis and with proper approvals, as powder for compacts or in the preparation of master alloys. In the processing of the 90-kg E-batch powder, 2.2 kg of oversize material were removed. The loss during blending and compacting of 15.5 kg of prepared E-batch powder was 20 g.

The materials balance for the arc melting of the E1 electrode and the preparation of the resulting E1 ingot for extrusion are shown in Table 9. The input consists of the alloyed electrode and the ingot pad used for the initial arc strike. The output consists of the ground ingot, the ingot pad, and stub, which are reusable in subsequent melts; additional recycled material; residuals from cutting and ingot grinding; and EB welding losses occurring during the filling of the shrinkage cavity in the ingot.

Table 9. Materials balance for E1 arc melting and ingot preparation

Type	Form	Weight (g)
	Input	
Virgin	Alloyed electrode	10,823
Recycle	Ingot pad	1,006
	Total	11,829
	Output	
Virgin	Ground ingot	8,496
Recycle	Ingot pad	1,577
Recycle	Electrode stub	954
Recycle	Ingot splatter	259
Residual	Cutting and grinding sludges	450
Loss	Electron beam welding and arc-melting losses	93
	Total	11,829

The extrusion and subsequent processing of the E1 ingot is not completed at this writing. Therefore, the processing of the D1 ingot is the most recent experience with these processing steps. The materials balance for the processing of the D1 ingot from extrusion through blank preparation is summarized in Table 10. The D1 extrusion is smaller than the E1 extrusion, although the results should be scaled appropriately for larger ingots.

Table 10. Materials balance for blank preparation from D1 extrusion

Type	Form	Weight (g)
	Input	
Virgin	Ground ingot	6,325
	Output	
Virgin	Blanks	2,172
Virgin	Test pieces	60
Recycle	Extrusion nose and tail and sheet skeletons	2,275
Solid scrap	Sheet trimming	686
Residual	Blanking and grinding sludges	918
Residual	Cutting sludges	214
	Total	6,325

The above results give an accurate analysis of the product and recycle outputs of the process. Determining the quantity of refinable scrap recovered as grinding and cutting sludges is not so direct or precise. Residues from cutting and grinding operations are recovered on a quarterly basis, and historical assays are used to estimate the quantity of iridium in the dry residue. The recovery of EB-melting residue is further complicated by the attachment of iridium residue to the liner. Some of this material is loosened and recovered when the liner is removed, and some remains as a deposit on the liner. No liner has been removed for recovery in the past two years, and the refining of a liner itself has never been shown to be economical because of the large amount of stainless steel and the small quantity of iridium. In order to estimate the fraction of the residual in each of these operations that is

recovered for refining and the quantity of material that is lost in the operation, we reviewed residual recovery data for the last production year, 1983, and also for the second and third quarters of 1988. Table 11 summarizes the fraction of iridium recovered for refining according to residual book value for these two years. The approximate average for the two years, shown in Table 11, was used to estimate the quantity of scrap produced from the residuals. The estimated iridium loss was then calculated as the difference between the residual value and the estimated iridium recovered as scrap. These are only approximations and must be verified by assaying and refining segregated scrap over a period of years of production. The approximate iridium loss for each operation is shown in the right column of Table 11 as a percentage of the iridium input to a virgin ingot. The single most important loss is in EB melting, followed by ingot grinding, EB welding, and blank electrodischarge machining. On the basis of this calculation, the estimated loss of iridium in the processing of a virgin ingot totals about 12% of the starting material, although the actual value may be higher.

Table 11. Summary of estimated residual scrap recoveries and losses

Operation	Estimate of recovered scrap (% of residual book value)			Estimated loss (% of total powder processed)
	Value for indicated year		Approximate average value	
	1983	1988		
Powder blending	0	0	0	0.2
Electron beam melting	40	45	45	6.1
Arc melting and cutting	75	64	70	0.4
Ingot grinding and cutting	NA	58	60	1.5
Electron beam welding	0	0	0	1.4
Extrusion cutting	76	96	85	0.3
Blank EDM	47	25	30	1.2
Blank grinding	84	96	90	0.6
Blank cleaning	0	0	0	0.1
		Total losses		11.8

An approximate materials balance for blank production can be calculated on the basis of the experience with the D1 and E1 ingots and the estimated recoveries from scrap residues. The results of such a calculation are shown in Table 12 for five categories of products: blanks, test pieces for product characterization, recycled material, scrap for refining, and unrecovered material or loss. The distribution of the products of the process is naturally sensitive to the yield of blanks at NDE and has been calculated for three levels of yield, with the 100% yield level shown as a basis for comparison. (This is a hypo-thetical level for delivery of flight-quality blanks, since some blanks are needed for test specimens.) The 85% yield level is the goal of the current process improvement program. The 70% level is the approximate yield obtained with the standard process for blank manufacture using drop-cast ingots. The distribution of products for processing virgin material without use of recycle is shown for the 100% NDE yield level, while the next column in the table indicates the distribution of products with complete use of recycled material, including recycle of

Table 12. Predicted materials balance for blank production: estimated distribution of process outputs for indicated NDE yields (% of net input)

Product	Virgin ingot 100% NDE yield	With complete recycle usage		
		100% NDE yield	85% NDE yield	70% NDE yield
Blanks	24	42	38	34
Test pieces	1	1	1	1
Recycle	38	0	0	0
Refinable scrap	25	41	44	47
Loss	12	16	17	18

nonflight-quality blanks. The estimates of material loss do not account for losses associated with refining. The use of recycle dramatically increases the quantity of blanks since EB melting, a high loss operation, is not required.

The material efficiency of the process can also be evaluated on the basis of number of flight-quality blanks per kilogram of iridium powder consumed. At a blank yield of 85% at NDE, a total of 12 flight-quality blanks per 1 kg of powder processed is expected, assuming full use of recycle. Achieving these levels of material usage requires minimizing grinding of

the ingot, as was the case for E1, and efficient layout of the blanks as was the case for the D1 sheets.

A quantitative comparison of material usage anticipated for the new process with that of the standard process has not been done. Qualitatively, the new process improves material usage by reducing the high level of edge cracking associated with rolling drop-cast ingots produced by the old process. A secondary benefit of the new process is the elimination of the molybdenum frames required to cross-roll ingots in the old process, which avoids the necessity of edge trimming the iridium sheet skeletons before recycling this material.

6. SUMMARY

6.1 DISCUSSION

The results of this work provide substantial evidence that most of the laminations, which cause rejection of finished blanks, originate in the arc-melted ingot. Ultrasonic tests show that the defects that cause laminations occur before the extruded bar is cut for rolling. The arc-melting experiments performed using stainless steel show that subsurface pores are not uncommon. The general correlation between the location of ultrasonic indications in the arc-melted ingot and the location of ultrasonic indications in the blanks produced from this ingot provides yet further confirmation.

The arc-melting development has shown that the existing consumable arc-melting furnace does not have adequate alignment control or arc-gap control to consistently produce the high-quality iridium alloy ingots necessary for a high yield of finished blanks. Purchase of a new arc-melting furnace with automated control of melt parameters, improved alignment, and improved arc-gap control has been authorized; this furnace is scheduled to be available in FY 1990. In the interim, alignment of the electrode should be controlled as closely as possible.

The results obtained with refinable scrap iridium and with stainless steel show that the melting of a 25-mm-diam electrode in a 51-mm-diam mold does not provide sufficient clearance to avoid arc strikes to the mold wall and resulting ingot surface defects. An increase in the mold diameter to 63 mm can dramatically improve the ingot surface quality.

In the past year the extrusions of iridium alloy ingots canned in molybdenum include the D1 ingot through a 19- by 51-mm die opening and two refinable scrap ingots (RS1 and RS2) through a 37.5-mm-diam die opening. All three extrusions were performed with

75-mm-diam extrusion billets preheated at 1325°C. The calculated extrusion K-factors are 700 MPa for D1 extrusion and 805 and 655 MPa for RS1 and RS2 extrusions, respectively. The lower value for RS2 as compared to D1 can be attributed to the fact that round extrusions usually exhibit lower K-factors than do rectangular or shaped extrusions. The high value for RS1 is not readily explained but may indicate that improved control of extrusion variables conditions is required.

6.2 RECOMMENDATIONS

The following recommendations can be made to improve the quality of arc-melted iridium alloy ingots in order to improve the yield of blanks:

1. Install and qualify a new consumable arc-melting furnace with improved electrode alignment and arc-gap control.
2. Increase the mold diameter from 51 to 63 mm in order to avoid arc strikes to the mold wall.
3. Continue to grind and ultrasonically inspect arc-melted ingots to determine the relationship of defects in the ingot to those in the blanks.
4. Continue monitoring of extrusion parameter and as-extruded microstructure to minimize variability in the extrusions.

7. ACKNOWLEDGMENTS

The encouragement and support of W. J. Barnett, DOE Office of Special Applications, are gratefully acknowledged. The authors wish to thank C. E. Dunn, G. E. Angel, K. S. Blakely, R. A. Cunningham, Jr., C. W. Holland, Jr., and J. D. Vought for their contributions to the experimental work. The authors also thank V. K. Sikka for useful discussions of this work; R. H. Cooper, K. V. Cook, and M. M. Martin for both discussions during the course of this work and internal review of the manuscript; M. L. Atchley and D. D. McCoy for typing the draft; C. I. Moser for editing; and D. L. Balltrip for preparing the manuscript.

8. REFERENCES

1. R. L. Heestand, G. L. Copeland, and M. M. Martin, *A Consumable Arc-Melting, Extruding, and Rolling Process for Iridium Sheet*, ORNL-6270 (1986).

2. R. L. Heestand, E. K. Ohriner, and T. K. Roche, *Advances in Iridium Alloy Processing in 1987*, ORNL/TM-10852 (1988).

ORNL/TM-11392
Distribution
Category UC-504

INTERNAL DISTRIBUTION

1-2. Central Research Library
3. Document Reference Section
4-5. Laboratory Records Department
6. Laboratory Records, ORNL RC
7. ORNL Patent Section
8-10. M&C Records Office
11. G. E. Angel
12. D. E. Bartine
13. C. R. Bieber
14. J. A. Carter
15. K. V. Cook
16. R. H. Cooper, Jr.
17. G. L. Copeland
18. D. F. Craig
19. W. S. Dritt
20. E. P. George
21-25. R. L. Heestand
26. J. M. Holladay
27. J. A. Horak
28. H. E. Kim
29. O. F. Kimball
30. J. W. Koger
31. M. M. Martin
32. J. R. Merriman
33-37. E. K. Ohriner
38. G. E. Proffitt
39. P. N. Rader
40. C. R. Riggs
41. A. C. Schaffhauser
42. V. K. Sikka
43. G. M. Slaughter
44. G. B. Ulrich
45. F. W. Wiffen
46. D. F. Wilson
47. A. D. Brailsford (Consultant)
48. H. D. Brody (Consultant)
49. D. P. Pope (Consultant)
50. M. L. Savitz (Consultant)
51. E. R. Thompson (Consultant)
52. J. B. Wachtman (Consultant)

EXTERNAL DISTRIBUTION

53. AIR FORCE WEAPONS LABORATORY/AWYS, Kirtland Air Force Base, NM 87117

M. J. Schuller

54. AMES LABORATORY, 242 Spedding Hall, Iowa State University, Ames, IA 50011

B. J. Beaudry

55. BATTELLE COLUMBUS LABORATORIES, 505 King Avenue, Columbus, OH 43201

C. A. Alexander

56-57. FAIRCHILD INDUSTRIES, 20301 Century Blvd., Germantown, MD 20767

R. T. Carpenter
E. A. Skrabek

58-59. EG&G MOUND APPLIED TECHNOLOGIES INC., P. O. Box 3000, Miamisburg, OH 45342

W. R. Amos
W. H. Smith

60-64. GENERAL ELECTRIC COMPANY, Astro-Space Division, P. O. Box 8555, Building B, Philadelphia, PA 19101

P. Gorsuch, 29B12-KB
V. F. Haley, 20B41-KB
R. F. Hartman, 29B12-KB
R. J. Hemler, 29B12-KB
J. R. Peterson, 29B12-KB

65-66. JET PROPULSION LABORATORY, California Institute of Technology, 4800 Oak Grove Drive, Pasadena, CA 91103

R. W. Campbell
R. J. Spehalski

67. JOHNS HOPKINS UNIVERSITY, Applied Physics Laboratory, Johns Hopkins Road, Laurel, MD 20810

J. C. Hagan

68-69. LOS ALAMOS NATIONAL LABORATORY, P. O. Box 1663, Los Alamos, NM 87545

T. C. Wallace, Sr.
R. W. Zocher

70. MICHIGAN TECHNOLOGICAL UNIVERSITY, Department of Metallurgical Engineering, Houghton, MI 49931

C. L. White

71. NUS CORPORATION, 910 Clopper Road, Gaithersburg, MD 20889

R. W. Englehard

72-73. ROCKWELL INTERNATIONAL, Rocketdyne Division, 6633 Canoga Avenue, Canoga Park, CA 93104

L. Auge
E. Baumeister

74. TELEDYNE ENERGY SYSTEMS, 110 W. Timonium Road, Timonium, MD 21090

P. Dick

75. THERMOPHYSICAL PROPERTIES RESEARCH LABORATORY, Purdue University, 2595 Yeager Road, West Lafayette, IN 47906

R. E. Taylor

76-77. WESTINGHOUSE HANFORD COMPANY, P. O. Box 1970, Richland, WA 99352

R. L. Knecht
M. J. Wiemers

78. WESTINGHOUSE SAVANNAH RIVER COMPANY, Bldg. 221-HBL, Aiken, SC 29801

C. R. Goetzman

79-83. U. S. DEPARTMENT OF ENERGY, Office of Special Applications, NE-53, GTN, Washington, DC 20545

W. J. Barnett
A. S. Mahner
A. L. Mowery
R. C. Raczynski
J. A. Turi

84-85. U. S. DEPARTMENT OF ENERGY, Albuquerque Operations Office, P. O. Box 5400, Albuquerque, NM 87115

C. Garcia
C. B. Quinn

86. U.S. DEPARTMENT OF ENERGY, Dayton Area Office, P.O. Box 66, Miamisburg, OH 45324

J. A. Morley

87. U.S. DEPARTMENT OF ENERGY, Richland Operations Office, P.O. Box 550, Richland, WA 95350

O. A. Farabee

88. U.S. DEPARTMENT OF ENERGY, Savannah River Operations Office, P.O. Box A, Aiken, SC 29801

C. R. Richins

89. U.S. DEPARTMENT OF ENERGY, Oak Ridge Operations Office, P.O. Box 2001, Oak Ridge, TN 37831-8600

Assistant Manager, Energy Research and Development

90-201. U.S. DEPARTMENT OF ENERGY, Office of Scientific and Technical Information, Office of Information Services, P. O. Box 62, Oak Ridge, TN 37831

For distribution as shown in DOE/OSTI-4500, Distribution Category UC-504 (Materials).

☆U.S. GOVERNMENT PRINTING OFFICE 1990--748-114/00130